Transportation Research Part C 155 (2023) 104311

Contents lists available at ScienceDirect

Transportation Research Part C

journal homepage: www.elsevier.com/locate/trc

I-24 MOTION: An instrument for freeway traffic science

Derek Gloudemans [a,b,*], Yanbing Wang [a,c], Junyi Ji [a,c], Gergely Zachár [a], William Barbour [a], Eric Hall [a], Meredith Cebelak [e], Lee Smith [d], Daniel B. Work [a,b,c]

[a] Institute for Software Integrated Systems, Vanderbilt University, Nashville, TN, United States
[b] Department of Computer Science, Vanderbilt University, Nashville, TN, United States
[c] Department of Civil and Environmental Engineering, Vanderbilt University, Nashville, TN, United States
[d] Traffic Operations Division, Tennessee Department of Transportation, Nashville, TN, United States
[e] Gresham Smith, Nashville, TN, United States

ARTICLE INFO

Keywords:
Vehicle trajectory data
Open-road testbed
Sensor network
Connected and automated vehicle testing
Computer vision

ABSTRACT

The Interstate-24 MObility Technology Interstate Observation Network (I-24 MOTION) is a new instrument for traffic science located near Nashville, Tennessee. I-24 MOTION consists of 276 pole-mounted high-resolution traffic cameras that provide seamless coverage of approximately 4.2 miles I-24, a 4-5 lane (each direction) freeway with frequently observed congestion. The cameras are connected via fiber optic network to a compute facility where vehicle trajectories are extracted from the video imagery using computer vision techniques. Approximately 230 million vehicle miles of travel occur within I-24 MOTION annually. The main output of the instrument is vehicle trajectory datasets that contain the position of each vehicle on the freeway, as well as other supplementary information such as vehicle dimensions and class. This article describes the design and creation of the instrument, and provides the first publicly available datasets generated from the instrument. The datasets published with this article contains at least 4 hours of vehicle trajectory data for each of 10 days. As the system continues to mature, all trajectory data will be made publicly available at i24motion.org.

1. Introduction

Transportation science is undergoing a digital transformation in which increasingly automated vehicles are being developed and deployed on roadways, changing the fundamental physics of traffic flow. Even a small number of automated vehicles can have a direct impact on the macroscopic behavior of traffic flow, highlighting the need to monitor and observe traffic flows across microscopic and macroscopic scales.

At the same time new vehicles are being introduced that may alter the flow, new technologies are advancing that ease the ability to capture the behavior of traffic at scales that were impossible to realize even a few years ago. For example, SAE level 1 and 2 automated vehicles with adaptive cruise control now transmit critical contextual data about the surrounding environment on the vehicle Controller Area Network (CAN), allowing opportunities to measure vehicle spacings and relative velocities, which were not possible using only Global Navigation Satellite Systems (GNSS) devices in phones and vehicles. Drone technologies have reached a degree of maturity that now facilitate camera based monitoring over roadways at impressive spatial scales. While these advancements offer opportunities to accelerate traffic flow science, there are still direct needs for monitoring the individual and collective behavior of vehicles over long temporal and spatial resolutions.

* Corresponding author at: Institute for Software Integrated Systems, Vanderbilt University, Nashville, TN, United States.
E-mail address: derek.gloudemans@vanderbilt.edu (D. Gloudemans).

https://doi.org/10.1016/j.trc.2023.104311
Received 10 February 2023; Received in revised form 9 August 2023; Accepted 16 August 2023
Available online 4 September 2023

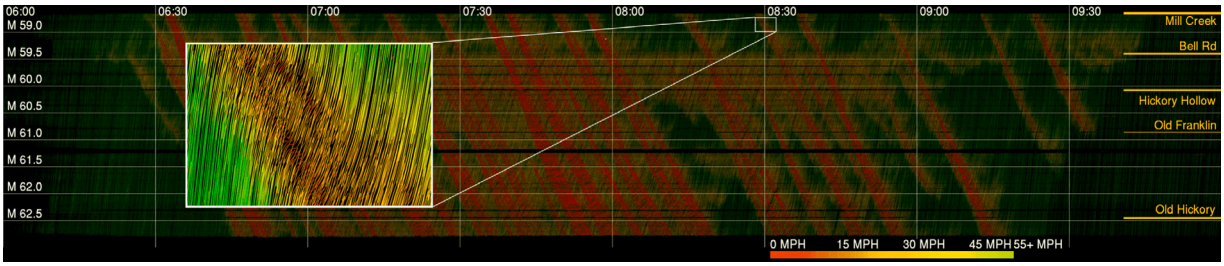

Fig. 1. Time–space diagram for four hours of I-24 W morning rush hour traffic on Nov 25, 2022, generated from I-24 MOTION vehicle trajectories. x-axis: time of day (HH:MM); *y*-axis roadway postmile (mi). Postmile decreases for travelers in the westbound direction. A typical congestion pattern is shown with frequent oscillatory traffic observed; and recurring waves travel upstream relative to the direction of traffic at 12–13 mph. The names of interchanges and overpasses appear on the right. The figure inset shows a zoomed in portion of the data which is 0.25 mi in length and 4 min in duration.

Table 1
Comparison of existing highway complete vehicle trajectory datasets. "~" indicates approximate value. "–" indicates data is not available.

Dataset	Location	Context	Year	Cameras	Time scale	Spatial scale	Vehicles
NGSIM US-101 (Alexiadis et al., 2004)	Los Angeles, CA	5-6 lane highway	2005	8	0.75 h	0.64 km	9,206
HighD (Krajewski et al., 2018)	Cologne, GE	2-3 lane highway	2018	1	16.5 h	0.42 km	110,500
ExiD (Moers et al., 2022)	Aachen and Cologne, GE	2-4 lane interchanges	2021	1	16.1 h	0.42 km	69,172
Automatum (Spannaus et al., 2021)	GE	2-4 lane highway	2021	1	30 h	0.66 km	60,000
HIGH-SIM (Shi et al., 2021)	I-75, FL	3-4 lane highway	2021	3	2 h	2.44 km	–
Zen Traffic Dataset (Seo et al., 2020)	Osaka, JP	2 lane highways	2018	–	5 h	~2 km	–
I24-MOTION (released)	Nashville, TN	4-5 lane highway	2022	276	47 h	6.75 km	~600,000
I24-MOTION (planned)	Nashville, TN	4-5 lane highway	2023	276	Daylight	6.75 km	~150,000/day

Recognizing the impact of freeway trajectory data collection efforts such as NGSIM (Alexiadis et al., 2004) and HighD (Krajewski et al., 2018) (see also Table 1), and emerging urban datasets exemplified by pNEUMA (Barmpounakis and Geroliminis, 2020), and at the same time the limited availability of sources for trajectory data, we started on a 5-year effort to instrument a section of freeway that could help enable the next wave of empirical traffic science that depends on abundant trajectory datasets. This article presents the outcome of that effort, resulting in an instrument known as I-24 MOTION.

I-24 MOTION is a camera-based trajectory generation system located on I-24 near Nashville, TN. The instrument consists of 276 4K resolution video cameras mounted on 40 poles ranging from 110 ft to 135 ft above the freeway. The cameras are positioned with overlapping fields of view and are connected by a fiber optic network to a compute facility where the videos are converted to vehicle trajectories. The instrument captures approximately 230 million vehicle-miles of travel annually, and experiences regular recurring congestion.

Fig. 1 illustrates the data captured by I-24 MOTION, showing a time–space diagram spanning 4.2 miles of I-24 westbound traffic during 4 h of morning congestion starting at 6:00 AM. The image is created by plotting all westbound vehicle trajectories and color-coding the points based on the speed of the vehicle. Vehicle lengths, widths, heights, and lateral positions are also measured but not shown. The waves visible in the image propagate at approximately 12–13 miles per hour. Data used to generate this diagram are released with this work.

The main contribution of this article is the creation of the I-24 MOTION instrument, which generates the trajectory datasets released with this work. The article provides the description of key elements of the instrument, including the road network geometry and features, the features of the cyber–physical assets that compose the instrument, and the general data processing steps. It also shares initial datasets and introduces the location for where future datasets will be released.

These elements of this article are critical to understand the uses and limitations of the current and future datasets. For example, as we explain in Section 3, the cameras are pole-mounted. The height of the poles are selected to minimize occlusion (excellent for generating accurate vehicle trajectories), but the height can allow sway in strong winds (bad for generating accurate vehicle trajectories). Thus, the physical design directly influences the types of artifacts that can be introduced. The datasets released by I-24 MOTION will be provisioned with a digital object identifier and change logs as new data processing algorithms are deployed and as artifacts are removed.

We also provide a preliminary description of the datasets, the known artifacts today, and our plans to improve them over time. It is clear that at a macroscopic scale, the data in the initial release can already support novel macroscopic analysis and insight, since no interpolation is required — all 4 miles are observed. At the same time, we describe known issues (e.g., fragmented trajectories due to tracking failures; fragmented trajectories due to a vehicle crash which damaged hardware on one pole, etc.). Some of these issues will be resolved through instrument maintenance cycles; while others will be resolved with the advancement of better automated data generation methods. As individual datasets mature, and new datasets are introduced, this article will serve as the reference point for users of all future datasets generated by the instrument.

The remainder of this article is organized as follows: Section 2 reviews the literature landscape around vehicle trajectory data, situating this work among existing research efforts. Section 3 describes the physical infrastructure, hardware, and software systems

of I-24 MOTION. Section 4 describes the data produced in more detail, including the recorded quantities, coordinate system, and a comparison in spatio-temporal scale to existing vehicle trajectory dataset. Section 5 provides some preliminary analysis of the data including a characterization of the wave propagation speeds observed in the datasets. Lastly, Section 6 highlights the future direction of the instrument.

2. Related work

2.1. Data collection for traffic modeling

At the macroscopic level, traffic phenomena are often observed and described with three quantities of interest, i.e., flow, speed, and density (May, 1990). Fundamental diagrams (Turner, 2011) like the Greenshields and Greenberg models (Greenshields et al., 1935; Greenberg, 1959) relate the traffic quantities while models such as the Lighthill–Whitham–Richards (LWR) (Lighthill and Whitham, 1955) and the Aw–Rascle–Zhang (ARZ) (Aw and Rascle, 2000) are developed to describe the spatio-temporal evolution of traffic. These models can be validated with data collected from radar-based devices and loop detectors (Roess et al., 2004). Large-scale macroscopic data monitoring systems such as the freeway performance measurement system (PeMS) (Choe et al., 2002) in the United States; the A5 freeway near Frankfurt (Schönhof and Helbing, 2007) in Germany; and the M42 highway (Stewart et al., 2006) in England; and later floating-vehicle measurement-based on cell phone carrier data (Bar-Gera, 2007) or GNSS positional data (Herrera et al., 2010) have enabled research on macroscopic traffic flow dynamics (Helbing, 1997; Helbing and Treiber, 1998; Kerner, 1999; Treiber et al., 2000; Zheng et al., 2011). A challenge is that the data typically must be interpolated spatially (in the case of inductive loops), or scaled up across all vehicles (in the case of probe data) to gain a complete spatio-temporal picture.

Unlike the accumulated average macroscopic data and models, microscopic models give attention to the interactions between individual vehicles. Since the early car-following experiments (Chandler et al., 1958) conducted by physically connecting vehicles to measure space gap, many emerging in-vehicle technologies including on-board radar detectors (Kesting and Treiber, 2008), cameras (Jones, 2001), laser sensors (Göhring et al., 2011) and GNSS devices (Gurusinghe et al., 2002; Ma and Andréasson, 2006) have been applied to measure vehicle spacing, speed and relative speed.

With the advances in visual sensing, video-based trajectory data from road-side cameras, high buildings, helicopters and drones gradually has become a mainstream source for microscopic modeling (Treiterer and Myers, 1974; Alexiadis et al., 2004; Ossen and Hoogendoorn, 2005; Ossen et al., 2006; Ossen and Hoogendoorn, 2008; Krajewski et al., 2018). Trajectory data with the complete information for specific road segments supported a range of efforts including the development, calibration and validation of car-following models (Tordeux et al., 2010; Koutsopoulos and Farah, 2012), lane-change modeling, trajectory prediction (Deo and Trivedi, 2018; Altché and de La Fortelle, 2017), and traffic oscillation analysis (Yeo and Skabardonis, 2009).

Some traffic phenomena benefit from observation of traffic across the micro and macroscopic scales. For example, traffic waves observable at the macroscopic scale can result from instabilities and disturbances in the flow at the level of individual vehicles (Treiterer and Myers, 1974; Laval and Daganzo, 2006). Macroscopic data, frequently used for traffic wave studies, can cover a great spatiotemporal scale that reveals the dynamics of traffic waves on road networks, but it is unable to provide insight into why the wave is generated and how it is propagated. Trajectory data can help provide these insights (Li et al., 2014; Laval and Leclercq, 2010; Zheng et al., 2011) when available with adequate spatiotemporal coverage. Hence, abundant trajectory datasets, as highlighted in the article (Li et al., 2020), can enable traffic research at both the macroscopic and microscopic scales, aiding in understanding traffic phenomena like jam clusters and state transition dynamics (Schönhof and Helbing, 2007; Kerner and Lieu, 2005; Seo et al., 2017). It can also capture the complex interaction within multiple-class traffic participants for heterogeneous traffic flow (Khan and Maini, 1999; Arasan and Koshy, 2005; Ambarwati et al., 2014).

2.2. Existing testbeds

I-24 MOTION also operates as an open road testbed, which allows experiments to be conducted on the freeway and measured using the instrument. Existing *closed course* and *open road* testbeds already address some critical emerging research needs (Emami et al., 2020). Closed course testbeds, such as the American Center for Mobility (American Center for Mobility, 2021), MCity (Briefs, 2015), GoMentum Station (Cosgun et al., 2017), and Suntrax (Heery et al., 2017), have the distinct advantage of being capable of hosting experiments and data collection for cutting edge technologies and techniques including those under active research and development. By testing in highly controlled settings, they can assure safety and eliminate external factors such as unpredictable drivers and road conditions that can confound experiments. Because of the motivating objectives of closed course testbeds, they can be limited in their ability to test in real traffic conditions with regular drivers encountered on public roads. Open road testbeds exist in many forms on a variety of road types; examples include the Minnesota Traffic Observatory (Parikh and Hourdos, 2014), The Ray (Ray C. Anderson Foundation, 2021), the California Connected Vehicle Test Bed (Farrell et al., 2015), Ann Arbor Connected Vehicle Test Environment (University of Michigan Engineering, 2021), and Providentia (Krämmer et al., 2019). They support experiments in live traffic, similar to the I-24 instrument. Currently, the collection of high-fidelity trajectory data on each and every vehicle on the roadway over a multi-mile scale does not exist the United States, though the Lower Saxony testbed and the Zen Traffic initiative support these objectives in Germany and Japan. Table 2 summarizes these existing vehicle testbeds.

Table 2
Existing vehicle testbeds. *DSRC* indicates direct short range communications, *Trajectories* indicates complete vehicle trajectory generation, *CV* indicates connected vehicle testing, *V2I* indicates vehicle to infrastructure testing, and *AV* indicates autonomous vehicle testing.

Testbed	Location	Sensors	Type	Intended Usage
ACTION (FHWA, 2022)	Tuscaloosa, AL	DSRC, Cameras	Open road	CV, V2I
M-City (Briefs, 2015)	Ann Arbor, MI	DSRC, Cameras	Closed course	AV
The Ray (Ray C. Anderson Foundation, 2021)	Interstate 85, GA	DSRC	Open road	CV, V2I
California CV Testbed (Farrell et al., 2015)	Palo Alto, CA	DSRC	Open road	CV, V2I
Gomentum (Cosgun et al., 2017)	Concord, CA	LIDAR, DSRC, Cameras	Closed course	CV, AV
ACM Proving Grounds (American Center for Mobility, 2021)	Ypsilanti, MI	DSRC	Closed course	AV
SunTrax (Heery et al., 2017)	Orlando, FL	DSRC	Open road	V2I
AACTVE (University of Michigan Engineering, 2021)	Ann Arbor, MI	DSRC	Open road	V2I
Providentia (Krämmer et al., 2019)	Munich, DE	Radar, Cameras	Open road	Trajectories
Minnesota Traffic Observatory (Parikh and Hourdos, 2014)	Minneapolis, MN	Radar	Open road	Trajectories
Lower Saxony Testbed (von Schmidt et al., 2021)	Braunschweig, DE	LIDAR, DSRC, Cameras	Open road	Trajectories, CV, AV
Zen Traffic Roadways (Seo et al., 2020)	Osaka, JP	Cameras	Open road	Trajectories, CV, AV
I-24 MOTION	Nashville, TN	Cameras	Open road	Trajectories, CV, AV

2.3. Emerging observation technologies

In a parallel thread, significant research has been devoted to the computer vision tasks of *object detection* (locating relevant objects within an image) and *object tracking* (associating distinct objects in video frames across time). Especially in the past 10 years, rapid progress has been made in the use of modern hardware (Krizhevsky et al., 2012), neural network architectures (He et al., 2016; Redmon et al., 2016; Girshick, 2015; Duan et al., 2019), and massive-scale image datasets (Deng et al., 2009; Lin et al., 2014) to fit accurate object detection algorithms. Approaches for extracting vehicle trajectory data utilizing these techniques have been proposed. For example, the work (Dubská et al., 2014b) proposes a method to detect vehicle 3D rectangular prism bounding boxes using background subtraction and blob segmentation, relying on automatic parameter extraction of the scene homography proposed in Dubská et al. (2014a). The work (Sochor et al., 2018) uses this data to train a *convolutional neural network* (CNN) to produce the same data without the need for scene-wide calibration. In Ren et al. (2018), 2D object detectors are used to estimate vehicle positions on the road plane (the ambiguity of vehicle position within a 2D bounding box is not fully addressed). Subedi and Tang (2019) uses ground plane projection of vehicle pixels from multiple cameras to estimate the vehicle's position, validating with turning movement counts. Other solutions rely on re-identification of 2D tracked objects, without addressing 2D annotation position ambiguity (Tang et al., 2018; Chen et al., 2019). Other methods utilize instance segmentation networks (Zhao and Li, 2019; He et al., 2017) on traffic scenes with little occlusion. A few approaches (Zhang and Jin, 2019; Malinovskiy et al., 2009) avoid object detection by measuring object presence in *longitudinal scanlines* along each roadway lane, but occlusion and lane changes pose difficult challenges in this problem formulation. In theory, such methods promise to address the shortage of trajectory data.

These advances, along with the increasing prevalence of aerial drones, have enabled recent research efforts to revisit the task of vehicle trajectory extraction and make marked advancements to the state of the art. The HighD, Krajewski et al. (2018), ExiD (Moers et al., 2022), AUTOMATUM (Spannaus et al., 2021), and HIGH-SIM (Shi et al., 2021) datasets all utilize aerial imagery shot from either drone or helicopter-mounted cameras to produce complete highway vehicle trajectory data, and the *Third Generation Simulation* (TGSIM) (James, 2023) is a similar in-progress effort designed to capture trajectory data containing deployed automated vehicle technologies. Similarly, the pNEUMA (Barmpounakis and Geroliminis, 2020), inD (Bock et al., 2020), rounD (Krajewski et al., 2020), OpenDD (Breuer et al., 2020), Interaction (Zhan et al., 2019) and CitySim (Zheng et al., 2022) datasets utilize drones or swarms of drones to study complex urban vehicle and pedestrian interactions in more detail. High aerial fields of view make modern image segmentation algorithms (He et al., 2017) well posed for vehicle tracking in these contexts, but these methods are temporally limited by the relatively short battery life of drones (generally under an hour) and the requirement for human pilots.

3. System description

This section describes the I-24 MOTION instrument, detailing the physical infrastructure, network and compute hardware, and core algorithms required to provide accurate and complete vehicle trajectory data across a large spatial and temporal scale. The system is still in active development, and continual improvements to improve the reliability, accuracy, and processing speed of the system will be made over the following years.

3.1. Physical infrastructure

The I-24 MOTION instrument provides a continuous field of view of 4.2 miles (6.75 km) on the 4-5 lanes (each direction) I-24 freeway, southeast of Nashville, Tennessee, USA. Pole mounted cameras are connected via a fiber network to a data center, as shown in Fig. 2, where computer vision tracking and trajectory processing takes place. A total of 276 4K resolution cameras are mounted on 40 poles, each 110–135 ft tall, spaced every 500–600 ft along the freeway. Thirty-four of the 40 poles house 6 cameras each, while 6 poles adjacent to interchanges instead house 12 cameras to provide expanded coverage. The poles provide an overhead

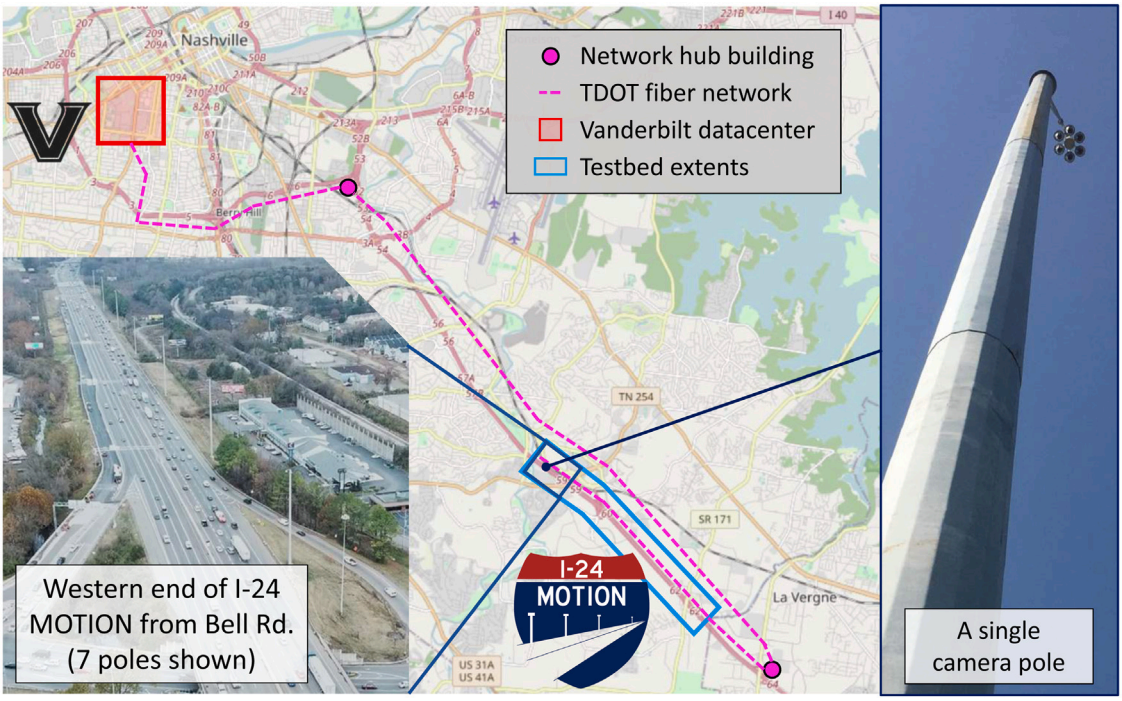

Fig. 2. Overview of I-24 MOTION site showing location relative to Nashville, TN. The major TDOT fiber network elements and their connection to Vanderbilt University, which houses the trajectory generation algorithms that operate on the live video feeds, are also shown on the map.

vantage point of the road to reduce occlusion, and to provide overlapping fields of view. (A separate 3-pole, 18 camera validation system (Barbour et al., 2020) is located about 0.75 miles eastbound on I-24 from the primary instrument and was used for technology testing and system planning).

3.1.1. Location

The location for I-24 MOTION was selected based on traffic conditions, constructability factors, and co-location with other *Tennessee Department of Transportation* (TDOT) initiatives. The four mile section of Interstate 24 is located ten miles southeast of Downtown Nashville and exhibits an *annual average daily traffic* (AADT) of approximately 150,000 vehicles per day across its length (Tennessee Department of Transportation, 2022). Morning and afternoon rush hour traffic exhibits reliably heavy congestion in opposite directions, frequently reaching stop-and-go conditions, with easily-observable traffic waves on a typical day. I-24 near Nashville is a heavy commuter and freight corridor (10%–15% of the vehicle traffic are heavy trucks): it links smaller cities of Murfreesboro, La Vergne, and Smryna with Nashville, and serves as a major shipping and industrial transportation route for Middle Tennessee and the southeast United States.

There are three highway interchanges in this section of I-24: Bell Road, Hickory Hollow Parkway, and Old Hickory Boulevard. Fig. 3 shows these three interchanges, their on/off ramps, and lane configuration; it also shows the placement of the forty poles with respect to these interchanges and other notable features on the roadway. The roadway elevation and grade is imposed below the roadway diagram in Fig. 3. The elevation and grade data was processed from aerial-based lidar measurements, conducted and published by the State of Tennessee (https://lidar.tn.gov). The processing of this data involved finding the best-fit piecewise second-order polynomial for the elevation data, then differentiating this polynomial to attain the piecewise linear grade function. This approach is consistent with the road design constraint for this roadway of allowing only constant or linear grade in the roadway profile. The elevation and grade data is included as metadata alongside the trajectory dataset.

This section of the I-24 corridor was also selected for the state's first *Integrated Corridor Management* (ICM) project, called the I-24 SMART Corridor, which operates on the 28-mile route between Nashville and Murfreesboro. The ICM project includes Interstate 24, the parallel arterial route SR 1, and connector routes between I-24 and SR 1. The ICM project has deployed an upgraded communications network and Intelligent Transportation System (ITS) devices, such as variable speed limit control, lane control, and ramp metering, for increased operational management of the corridor. This collocation will eventually allow the study of a variety of implemented ITS solutions associated with the I-24 SMART Corridor using I-24 MOTION (Chen and Ahn, 2015; Papageorgiou et al., 2003), when the active traffic management systems are enabled.

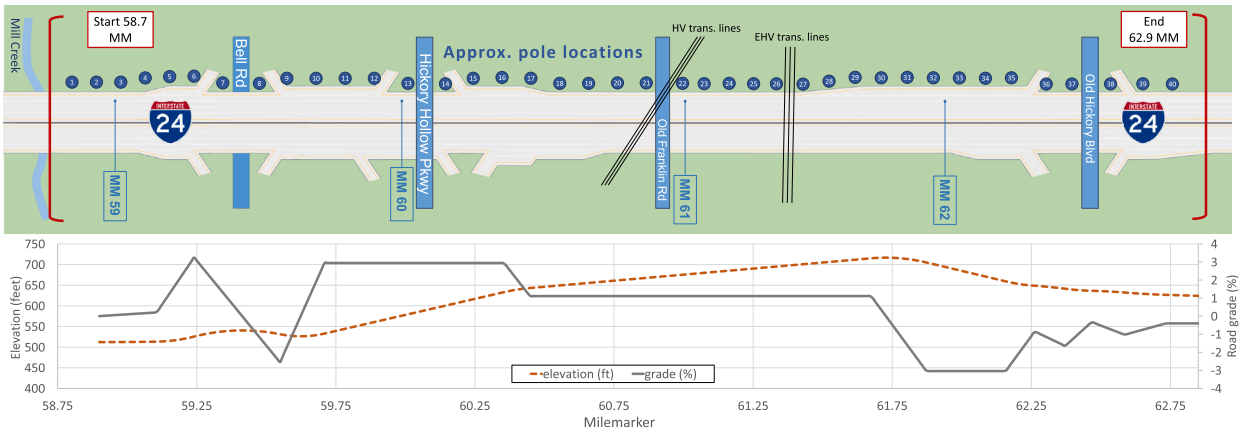

Fig. 3. TOP: Diagram of the I-24 MOTION instrument, spanning from Mill Creek (postmile 58.8) to milemarker 62.8. Camera poles (blue circles) are spaced at roughly 550-foot intervals and are shown in the image relative to other key infrastructure elements. The system spans three overpasses and one underpass, as well as three interchanges with 13 entrance/exit ramps. Relative positions of all elements are correct but diagram is not drawn to scale. **Bottom:** Elevation and road grade along the freeway. Grade is measured in the eastbound (diagram left to right) direction and was determined by differentiating the best-fit second-order piecewise polynomial elevation function.

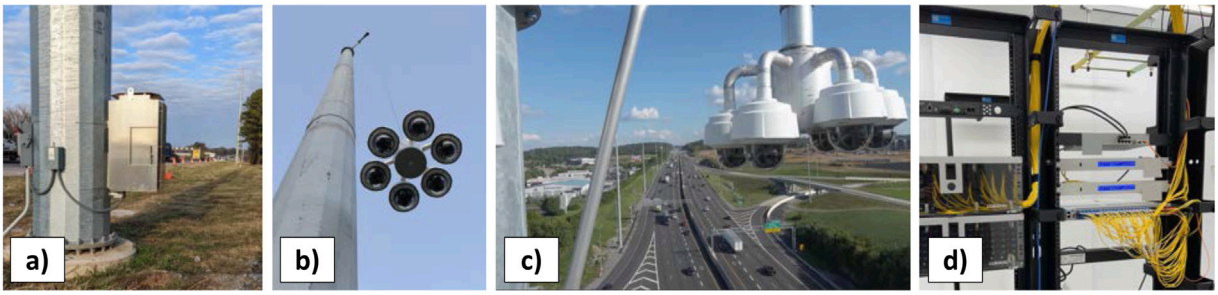

Fig. 4. Testbed components: (a) view of a camera pole base showing the electrical disconnect, transformer, and ground cabinet; (b) camera cluster in the process of lowering to the ground with the CLD; (c) view of camera cluster at the top of a pole; (d) fiber optic junction at network hub building and GNSS network time servers.

3.1.2. Camera poles

The 40 I-24 MOTION camera poles are each composed of a steel pole structure, ground-level communications and power cabinet, camera lowering device at the top of the pole, and custom camera cluster assembly, each detailed below. Fig. 4 shows select system components. Camera pole locations, as well as various other landmarks of interest, are included in Appendix A.

The camera pole system was prototyped across three years at existing pole locations on the TDOT network and with a purpose-built three-pole validation system constructed in 2020 (Gloudemans et al., 2020; Barbour et al., 2020). Valuable lessons from the validation system regarding camera selection, camera cluster mounting position, and pole-to-pole spacing were incorporated in the full system design. The details of the pole components are as follows:

- **Steel pole structure:** To observe all vehicles on the roadway with minimal occlusion, the poles are significantly taller than standard 30–50 ft poles used on many other CCTV systems. New poles and corresponding foundations were designed and built to a standard that the total deflection at the top of the pole is less than 1.5 inches in a 30 mph wind. Average pole-to-pole spacing is 550 ft across the instrument, with a minimum of 425ft and a maximum of 625ft due to roadside obstacles and entrance/exit ramps.
- **Ground-level cabinet:** A pole-mounted cabinet (shown in Fig. 4a) houses a network switch for the fiber optic network, a fiber patch panel, and two power supplies. Power supplies in the cabinet provide DC power to the fiber network switch in the cabinet (65 W supply) and to the camera cluster at the top of the pole (240 W supply). A fiber communications backbone is present throughout the instrument and links each pole to a communications hub building (shown in Fig. 4d) and the rest of the TDOT network. Each pole maintains a one gigabit per second network link to an aggregation network switch in a star network topology. This network topology helps simplify configuration and troubleshooting and has additional resilience in the case of some physical damage scenarios.
- **Camera lowering device:** The *camera lowering device* (CLD) is a critical component of all traffic monitoring cameras in the instrument. It allows the camera cluster to be safely lowered to the ground (see Fig. 4b) for routine cleaning and maintenance

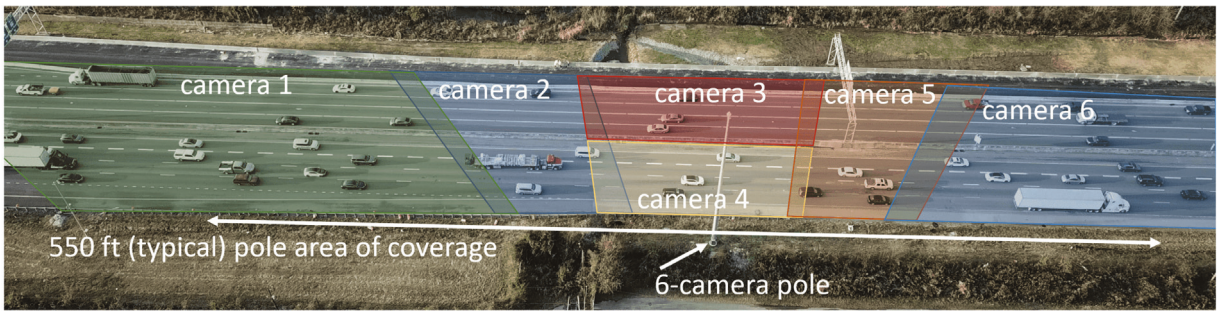

Fig. 5. Example camera fields of view for a single 6-camera pole. Each portion of the roadway is covered by at least one camera, with overlaps long enough to allow objects to be tracked between cameras.

using a winch at the base of the pole. While typically configured for only a single camera on a CLD, manufacturer collaboration and internal bench testing confirmed that the lowering device could support simultaneous data transmission from six 4K resolution video cameras to the ground-level cabinet where it ties into the fiber network. The CLD also contains redundant ethernet and power connections that can be utilized without the need for physical access to the top of the pole in case of a connector failure. The CLD is mounted to the top of the pole with a 54-inch extension arm and angled support strut (shown in Fig. 4c) for added rigidity.

- **Camera cluster assembly:** Mounted on each pole is a custom, 6-camera mount attached to the camera lowering device (shown in Fig. 4c). The orientation of the camera cluster is orthogonal to the roadway direction(s) of travel. The weather-tight camera mount holds a network switch which aggregates six video data streams to transmit them through a single gigabit ethernet connection on the CLD. The network switch receives DC power from the pole cabinet and supplies power over ethernet (PoE+) to each of the six cameras at 25.5 W. On the six poles adjacent to the three interchanges within the instrument, a second camera cluster assembly is mounted in an orientation pointing towards the under/overpass; in the future these cameras will support trajectory generation for vehicles as they enter and exit the highway.

3.1.3. Video cameras

The cameras on the instrument are a 4K resolution pan/tilt/zoom (PTZ) network IP model, powered by power over ethernet. The PTZ capabilities allow remote alignment to achieve the necessary 180-degree overlapping field of view across cameras on each pole, as seen in Fig. 5, and between camera poles. Deploying multiple cameras to each pole extends coverage of the instrument and reduces the number of poles needed. While cameras with wider image field of view exist, these suffered in testing from distortion at the edges of the image that could not easily be corrected to the accuracy needed for coordinate localization.

A critical technical consideration with network IP cameras is time synchronization across cameras and true frame capture time reporting. Cameras are synchronized over *network time protocol* (NTP) to a primary and secondary stratum 1 GNSS-based time servers on the local network (in the network hub building) and frequently re-synchronize (roughly every 15 min). The camera firmware provides timestamps associated with video frames corresponding at about 10 microsecond accuracy relative to the camera clock time. Cameras capture up to 4K resolution video at 30 frames per second. Frame-to-frame timing is typically observed to be uniform (33.3 ms), but in some cases non-negligible time differences result from duplicated or skipped frames (an artifact of camera exposure requirements as implemented in camera firmware.) Although the camera clocks are precisely synchronized and the exact frame capture times are different for all devices, accurate time-stamping of each frame allows processing algorithms to compensate for the relative time offsets for each camera.

3.2. Network and compute hardware architecture

All video data feeds are received from the TDOT network into a Vanderbilt data center for processing across a dedicated 40 gigabit fiber network connection. Centralized computing in a data center provides the computing hardware with dedicated, long-term support and infrastructure, in addition to future expansion possibilities. Two network switches support the cluster of servers: a data layer switch with two 25 gigabit connections to each server and a management layer switch for 1 gigabit user connectivity, control, and IPMI. A system control server directs the processing functions of the cluster across ten or more servers/nodes. It hosts a control interface where system managers dispatch processing jobs and propagates job configurations to each node. Nine processing nodes are dedicated to computer vision tracking and the initial trajectory construction. Each node contains eight graphics processing units (GPUs) that decode incoming video and perform object detection and tracking tasks. The nodes track vehicles across cameras, but each node operates independently with statically-assigned cameras. A vehicle traversing the entire instrument will generate a partial trajectory fragment on each of the (nine) processing nodes. Incoming video is buffered on its respective compute node and discarded after processing. Following initial trajectory generation, a post-processing server performs the complete trajectory assembly and reconciliation tasks. The cluster contains two data storage arrays responsible for storing the resulting trajectories – both initial trajectory fragments and post-processed complete trajectories – as well as log messages, monitoring data, algorithm training data, and instrument experiment data. Additionally, two servers within the cluster serve as a development and testing environment for new software versions and one server performs ancillary tasks such as large-scale visualization and traffic analysis.

Table 3
Data attributes for a single vehicle trajectory. Square brackets indicate an array of values.

Attribute	Type	Unit	Description
_id	12-byte BSON	–	Vehicle identifier unique across all I-24 MOTION data
Vehicle class	int	–	*0: sedan, 1: midsize, 2: pickup, 3: van, 4: semi, 5: truck, 6: motorcycle*
First timestamp	float	s	Minimum unix timestamp for this trajectory
Last timestamp	float	s	Maximum unix timestamp for this trajectory
Timestamp	[float]	s	Array of times at which vehicle positions are recorded
x position	[float]	ft	Array of longitudinal positions on roadway corresponding to each timestamp
y position	[float]	ft	Array of lateral positions on roadway corresponding to each timestamp
Starting x	float	ft	Longitudinal position on roadway at first timestamp
Ending x	float	ft	Longitudinal position on roadway at last timestamp
Length	float	ft	Vehicle length
Width	float	ft	Vehicle width
Height	float	ft	Vehicle height
Direction	int	–	−1 if westbound, 1 if eastbound
Configuration ID	int	–	Identifier linking data to a unique metadata indicating trajectory generation algorithm settings

3.3. Software architecture

A prototype software architecture comprises of three main modules: video ingest, vehicle detection and tracking, and trajectory post-processing and reconstruction, managed by the system control server. Before a run session starts, related configuration files and metadata are registered and stored in database for record-keeping or re-processing.

3.3.1. Video ingestion and recording

The cameras produce a H.264 encoded video, currently at 1080p resolution and 30 frames per second to reduce the data size. The streams are split into 10 min chunks and recorded into a Matroska (MKV) container. The timestamps, corresponding to the exact exposure moment of each frame (streamed separately in a custom field) which are incorporated into the PTS (Presentation timestamp) metadata during recording. This field is mandatory for video files, thus providing a standardized method for frame timing information, and enables interoperability with any conforming software. The video stream, with the current configuration and all 276 cameras, occupies ∼1 TB for each recorded hour at 1080p resolution.

3.3.2. Vehicle detection and tracking

Vehicle detection and tracking is performed using *Crop-based Tracking*, a joint detection and tracking method (Gloudemans and Work, 2021). This method processes only cropped portions of each overall image, drastically reducing detection inference time relative to processing each frame fully. Implicit in the use of this method is an accurate object motion model; object priors from this motion model are used to produce cropping boxes for each object, and only crops are processed by the object detector on most frames. We use a Retinanet (ResNet-50 backbone) object detector (Lin et al., 2017) to detect car and truck classes as listed in Table 3. Motorcycles are not currently detected but may be added in future work. For the motion model, a Kalman filter with linear dynamics is used. Objects are assumed to travel with constant velocity along the primary direction of roadway travel, and are assumed to have zero velocity perpendicular to the primary roadway direction (note that this motion constraint is relaxed during data postprocessing and is only used during initial object tracking). The intersection-over-union metric is used to compute affinity between object positions and new detections (Bochinski et al., 2017). IOU is computed based on vehicle footprints in space rather than bounding box coordinates within an image, which allows detections from multiple cameras with distinct fields of view to be incorporated provided accurate homography information is available for each camera (for more information on camera homographies and data coordinate system, see Section 4.2. The multi-camera tracking problem is solved by detection fusion (as in Strigel et al. (2013), Luna et al. (2022)) rather than trajectory fusion (as in Wu et al. (2019)) to reduce redundant tracking of the same object in multiple fields of view. Fig. 6 shows the result of object detection and tracking within image coordinates, and the corresponding roadway coordinate object positions obtained using image homography.

The complete set of 276 camera fields of view is subdivided across multiple processing nodes. On each node, all cameras are processed together (that is, roughly one frame from each camera is processed at a time, subject to some frame skips to keep cameras tightly time-synchronized). Processing nodes are not synchronized, so a single object traveling through the full instrument extents will be tracked as a separate vehicle with a unique ID on each processing node. This decouples the computation and allows the system to scale gracefully with a large number of cameras.

3.3.3. Trajectory post-processing

Although raw trajectory data from dense deployment of cameras and CV algorithms can achieve complete spatial and temporal coverage of a roadway segment, such data contains inaccuracies from camera errors (dropped, doubled, and corrupted frames) network errors (data packet drops), object detection and tracking (fragmentations, ID swaps, false negatives and false positives (Bernardin and Stiefelhagen, 2008)) often caused by object–object or infrastructure-object occlusions, timestamp quantization errors, homography assumption errors, and infeasible derivative quantities resulting from finite difference approximation over very

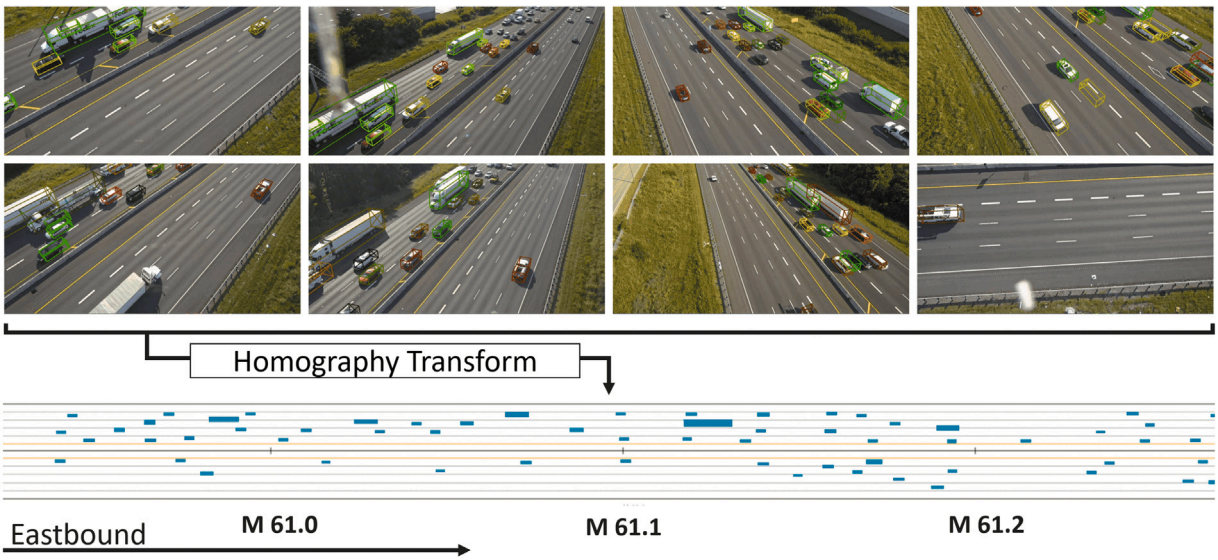

Fig. 6. Vehicles are represented as 3D rectangular prism objects (various colors above) using object detection algorithms within each camera frame. The resulting detected objects are transformed into roadway coordinates shared among all cameras, and tracked in this unified coordinate system. Each blue rectangle in the projected 2D birds-eye view represents a vehicle position.

short timescales. Treatments for specific sources of errors that rely on multiple iterations of rectification or require manual fine-tuning are not viable for longer term streaming datasets the I-24 MOTION is designed to produce. For small datasets, data cleaning and rectification with some manual involvement can address many common errors created in vehicular datasets (Coifman and Li, 2017).

I-24 MOTION uses an automatic data post-processing pipeline (Wang et al., 2022) which will be continuously improved to automate as much of the data cleaning steps as possible. Currently, it consists of (a) an online data association algorithm to solve a min-cost flow problem, which consequently matches fragments that belong to the same object, and (b) a trajectory reconciliation algorithm, which is formulated as a quadratic program. This algorithm reconstructs realistic vehicle dynamics from disturbed detection data with trajectory derivative smoothing and outlier correction while minimally perturbing the original vehicle detections. The resulting trajectories automatically satisfy the internal consistency (differentiation of trajectories with speeds and accelerations). Future post-processing development will consider conflict resolution along with trajectory smoothing to produce feasible inter-vehicular distances for accurate microscopic traffic studies, and may be able to leverage complementary efforts in trajectory prediction (Bahari et al., 2021).

4. Trajectory data

This section provides an overview of the data created by the I-24 MOTION system: its attributes, scale, conventions and coordinate system, known artifacts in the data, and a preliminary analysis of data accuracy.

4.1. Data description

One single continuous recording session on the I-24 MOTION instrument processed through the software pipeline (from Section 3.3) results in a vehicle trajectory dataset. Each dataset produced by the system consists of a collection of individual vehicle trajectories. An individual vehicle trajectory consists of vehicle attributes as well as motion information (see Table 3). Trajectory positions record the 2D footprint of the back center of each car, and are re-sampled at a frequency of 25 Hz to allow exact timestamp-based indexing. Derivative quantities such as velocity, acceleration and steering angle can be directly computed with position information via, for example, finite difference. An example vehicle trajectory is included in Appendix B.

Accompanying this work, 10 days of trajectory data are released from weekday morning traffic. Each dataset spans typically 4 h, from 6:00 AM to 10:00 AM, covering morning rush hour conditions. (Data from Friday, November 25th instead covers 11 h.) A variety of traffic conditions are present throughout the various days of data, including at least three crash-induced bottlenecks, one debris-induced bottleneck, high-traffic conditions with traveling waves, and free-flow traffic conditions. Table 4 summarizes the data released with this work. Additional metrics, statistics, time–space diagrams, and useful information can be found with the data release, as this information will change as the data is updated in future versions. Time–space diagrams for the westbound portion of the roadway on each day of trajectory data are included in Appendix C. Details on the data release are included in Section 4.5. Weather data for the days of this data release can be obtained from the *National Weather Service* (NWS) at https://www.weather.gov/wrh/Climate?wfo=ohx or *National Oceanic and Atmospheric Administration* (NOAA) at https://data.noaa.gov/onestop/.

Table 4
Details of the released dataset. "ID" indicates the unique dataset identifier used to associate all data and metadata for this dataset. Additional summary and statistic information is included with the data release.

Date	Day	ID	Start time (AM)	Duration (hours)	Notes
Nov 21, 2022	Monday	637b023440527bf2daa5932f	6:00	4	Crash, debris induced bottleneck
Nov 22, 2022	Tuesday	637c399add50d54aa5af0cf4	6:00	4	–
Nov 23, 2022	Wednesday	637d8ea678f0cb97981425dd	6:00	4	Crash
Nov 24, 2022	Thursday	637f0d5f78f0cb97981425de	6:00	4	Low traffic volume (holiday)
Nov 25, 2022	Friday	6380728cdd50d54aa5af0cf5	6:00	11	Low traffic volume (holiday)
Nov 28, 2022	Monday	638450a3dd50d54aa5af0cf6	6:00	4	Stopped vehicles induced slowdown
Nov 29, 2022	Tuesday	63858a2cfb3ff533c12df166	6:00	4	–
Nov 30, 2022	Wednesday	6386d89efb3ff533c12df167	6:00	4	–
Dec 1, 2022	Thursday	63882be478f0cb97981425df	6:00	4	Merge induced slowdown
Dec 2, 2022	Friday	63898d48d430891009401330	6:00	4	Crash

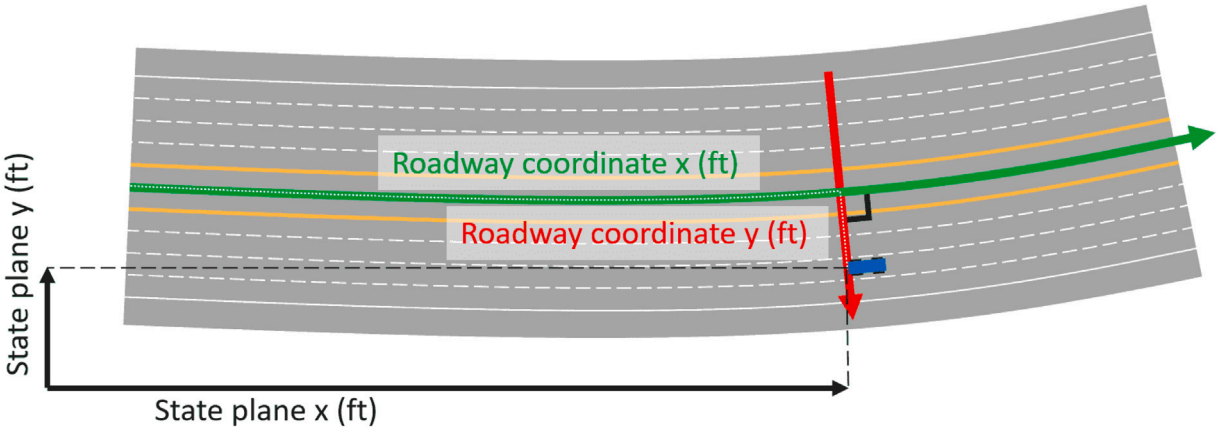

Fig. 7. Spline-curvilinear x-axis (green) and locally perpendicular y-axis (red) for roadway coordinates. State plane coordinates are shown in black for comparison. Position of the vehicle can be expressed either in state plane coordinates (black dashes) or roadway coordinates (white dots).

4.2. Data coordinate system

Data is provided natively in a curvilinear 2D roadway coordinate system, with the primary (x) axis aligned along the interstate roadway median and the secondary (y) axis defined locally perpendicular to the primary axis. This means that x is roughly equivalent to station or mile marker along the roadway, while y gives lateral or lane-position data. A second-order spline defines the x-axis in global (state plane) coordinates. (Control points for the center-line in state plane coordinates are included in metadata). This allows for the direct conversion of roadway coordinates into state plane coordinates, with a trivial conversion from state plane coordinates to GNSS WGS84 coordinates. Both coordinate directions are stored natively in feet. The positive x-direction is defined in the eastbound direction (direction of increasing post-mile as defined by the Interstate 24 mile markers), and x-coordinates are offset such that the x-coordinate for post-mile 60 corresponds exactly to $5280\times60 = 316800$ ft. (Other postmiles are approximately but not exactly located in this way (e.g. post-mile 61 $\approx 5280\times61 = 322080$ ft.) Adopting the left-hand rule convention, the y-coordinate is positive on the eastbound side of the roadway (vehicle is moving in increasing x-direction). Fig. 7 illustrates the coordinate system.

The primary advantages of a curvilinear coordinate system are twofold: *i.*) The coordinate system aligns lateral (lane position) information along the y-axis, while accounting for the longitudinal curvature of the roadway and aligning the direction of travel with the x-axis. *ii.*) A perpendicular slice of the roadway has a uniform x-coordinate.

While definition of the y-axis as locally perpendicular to the x-axis does allow for the same point to have multiple (x, y) locations, for reasonable roadway curvatures these points occur suitably far from the roadway surface where the coordinate system is relevant. This coordinate system also slightly underestimates the distance traveled (and therefore the instantaneous speed) of vehicles on the exterior of a curve, relative to vehicles on the interior of a curve. the magnitude of this effect is no more than the ratio of roadway width to radius of curvature, which tends to be small (less than 5%) on typical roadways. Exact distances traveled and speeds can instead be calculated by converting positions into state plane coordinates followed by finite difference calculation. Precise roadway geometry including lane marking coordinates will be made publicly available in a future work.

4.3. Positional accuracy

To assess the accuracy and suitability of I-24 MOTION trajectory data for micro-scale traffic analysis, output trajectory data is compared against an internal, manually labeled ground truth trajectory dataset, and onboard GNSS information from instrumented vehicles traveling on the roadway.

Table 5
Multiple object tracking and trajectory feasibility metrics for two ground truth scenarios (congested and free flow).

Metric (1.0 best)	Congested	Free-flow	Description
MOTA	0.93	0.93	Aggregate object tracking metric
MOTP (IOU)	0.73	0.72	Average precision (IOU) of matched object positions
Precision	0.98	0.97	Proportion of detected object positions matched to a ground truth position
Recall	0.95	0.96	Proportion of ground truth object positions matched to a detected object position
GT Match Rate	0.97	0.98	Proportion of ground truth trajectories matched to at least one detected trajectory
Pred Match Rate	0.99	0.76	Proportion of detected trajectories matched to at least one ground truth trajectory
Per GT Recall	0.91	0.95	Average proportion of a ground truth trajectory with correctly matched detected object positions
Per Pred Precision	0.98	0.74	Average proportion of detected trajectory correctly matched to a ground truth object
Feas. Accel.	1.00	1.00	Proportion of finite difference accelerations that are feasible (<10 ft/s^2)
Feas. Heading Angle	0.98	1.00	Proportion of finite difference heading angles that are feasible (<30°)
Feas. Direction	0.99	1.00	Proportion of finite difference velocities with correct magnitude (no backwards movement)
Feas. Overlapping	0.98	1.00	Proportion of detected trajectories that never overlap with another trajectory

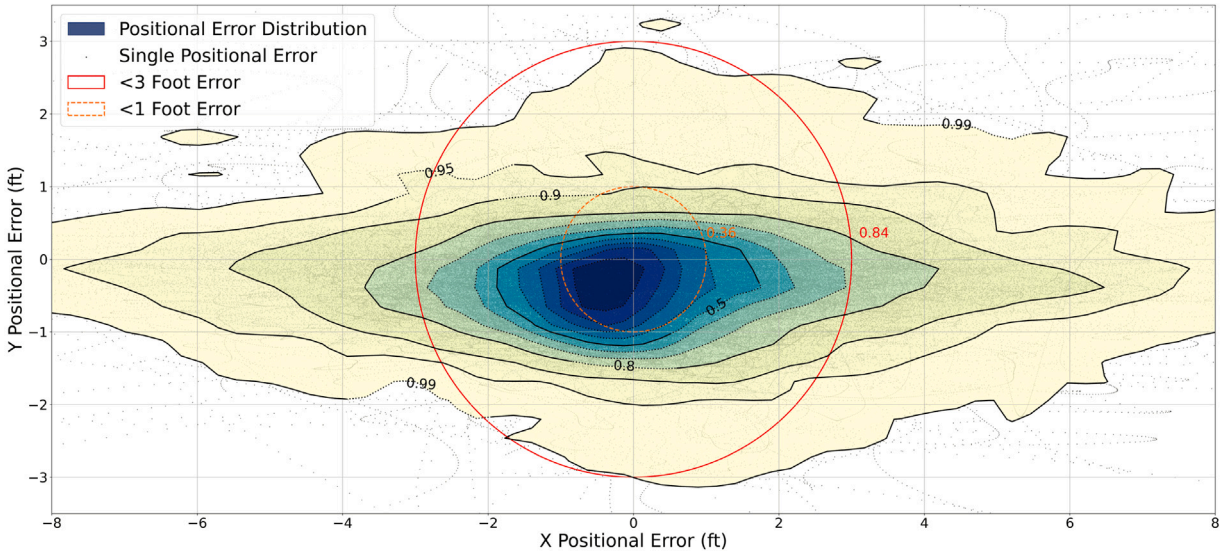

Fig. 8. Positional error histogram for trajectory data relative to ground truth trajectories. Contours show the proportion of data is contained within, and are at intervals of 0.1 unless otherwise indicated. Single positional errors are shown as black dots. A red circle shows the proportion of data with less than 1-meter positional error (0.87) and an orange circle shows the proportion of data with less than 1-foot positional error (0.36).

4.3.1. *Manually labeled ground truth*

Manual labeling of vehicles as 3D rectangular prism bounding boxes within videos from a subset of 18 cameras was performed for two scenarios: a free-flow traffic scenario and a highly congested (one side of roadway) scenario (Gloudemans et al., 2023a). In total, over 600,000 individual vehicle positions were labeled manually. The resulting vehicle trajectories were compared against the trajectory data output by running the I-24 MOTION trajectory generation algorithms on the same video data. For comparison, object positions were matched to *ground truth* (GT) object positions as in Berclaz et al. (2009) at each timestep. A minimum *intersection-over-union* (IOU) between the detected and ground truth vehicle position was required to consider the detected vehicle position a match for that ground truth object. Table 5 reports a number of multiple object tracking metrics for each scenario, as well as some metrics indicating the physical feasibility of the output trajectories. 97%–98% of ground truth objects have at least one detected trajectory assigned to them (GT Match Rate) and for ground truth objects, on average 91%–95% of the overall trajectory is covered by matching detected vehicle positions (Per GT Recall). Moreover, all vehicle accelerations produced by I-24 MOTION are physically feasible (< 10 ft/s^2), only 0%–2% of vehicle observations have infeasible heading angles, and only 0%–2% of vehicle trajectories overlap with another trajectory at some point.

For matched vehicle positions, Fig. 8 shows the relative error between the detected and ground truth vehicle position. 84% of detected vehicle positions fall within 3 ft of the ground truth position, and 36% fall within 1 foot of the corresponding ground truth. Table 6 reports the relative error between the detected and ground truth vehicle dimensions. All dimensions have a mean absolute error of less than 1.2 ft.

4.3.2. *GNSS data*

Trajectory data was compared against onboard vehicle GNSS sensor data, a commonly used sensor modality for obtaining single vehicle trajectories. GNSS-equipped vehicles were driven in eastbound and westbound lanes of traffic on the I-24 MOTION

Table 6
I-24 MOTION vehicle position and dimension errors relative to matched ground truth vehicles.

Quantity	Mean error (ft)	Standard deviation (ft)	Mean absolute error (ft)
Longitudinal (X) Position	0.2	2.6	1.7
Lateral (Y) Position	−0.3	0.6	0.6
Length	−0.6	2.5	1.2
Width	0.1	0.5	0.3
Height	0.5	0.8	0.7

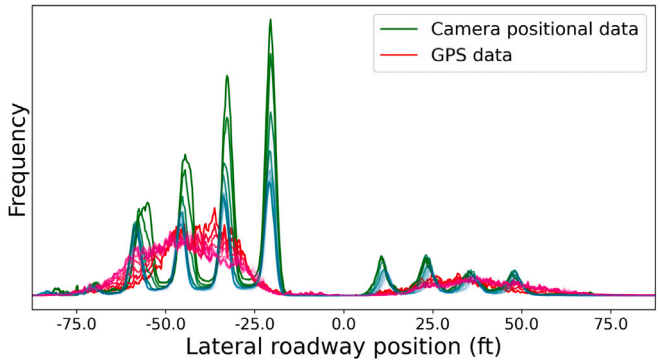

Fig. 9. Lateral position histogram aggregated over several 1000-foot longitudinal slices, for I-24 MOTION camera trajectory data (blue-green) and onboard GNSS data (pink-red). Strong peaks I-24 MOTION camera positional data correspond to lanes of travel. Data produced during AM rush-hour (higher traffic volume on westbound, negative lateral position, side of roadway).

instrument (Bunting et al., 2021). Over 600 vehicle runs through the instrument extents were conducted. Regular (1 s) positional data for each vehicle run was recorded. The reported *circular error probable* (CEP) for the sensor was 2.5 m. Fig. 9 shows a histogram of lateral positional data for each sensor modality (I-24 MOTION and GNSS data), aggregated for several longitudinal slices along the instrument. The I-24 MOTION data shows strong lateral peaks corresponding to vehicle presence in a specific lane of travel, whereas the GNSS lateral positional data does not show this characteristic. This is a strong indicator that I-24 MOTION yields strong lane-positional data, whereas this data is not necessarily available from an onboard GNSS sensor without heavy filtering. Due to this noisy lateral GNSS sensor data and the relatively high GNSS device error (2.5 m CEP), we prefer the manually labeled vehicle trajectories over GNSS sensor data for validating the quality of I-24 MOTION trajectory accuracy.

4.4. Data artifacts

Relative to previous complete vehicle trajectory datasets, the data and instrument proposed in this work offer new challenges to perfect the data. Previous works were conducted in areas of sufficiently small spatio-temporal scale that physical occlusions could mostly be avoided (by overhead vantage point and careful roadway segment selection). Moreover, they were of sufficiently small temporal scale that errors remaining in the data after trajectory generation could be removed with manual efforts (Coifman and Li, 2017). This approach is not scalable to the I-24 MOTION data, and some errors will always remain in the final data regardless of the algorithm employed. Enumerated here are a number of known errors in the initial data release that are artifacts of system hardware and software errors. We intend to partially or fully address each of these artifacts; moreover, open communication with I-24 MOTION data users will be maintained such that systematic errors in data creation can be addressed and data quality can be iteratively improved over time.

Fig. 10 shows time–space data with each type of data artifact present. Known data artifacts include:

- **Missing Pole:** Data from a single pole is occasionally missing from one of two sources. Brief outages can occur due to network communication issues. or to physical hardware damage (a camera pole was hit by a car in the week prior to most of the data in this work being generated). This manifests as a horizontal band on the time–space diagram (a contiguous spatial range of data missing across all recording time). Such issues are rare because poles are protected by guardrails, but these issues cannot be eliminated entirely.
- **Overpass Occlusion:** Overpass occlusion results in lost tracked vehicles, which also manifests as a contiguous spatial range of data missing across all recording time. This artifact will be addressed with an intelligent data processing step that matches objects disappearing under bridges with objects reappearing on the other side.
- **Static Homography Errors:** Initially, homographies for each camera were statically defined. However, pole deflection due to temperature and sunlight cause subtle shifts in camera positions. This manifests in very narrow (a few feet wide) horizontal bands on the time–space diagram that contain missing or doubled trajectory positional data. This issue will be corrected by periodically accounting for subtle camera motion by re-defining homographies.

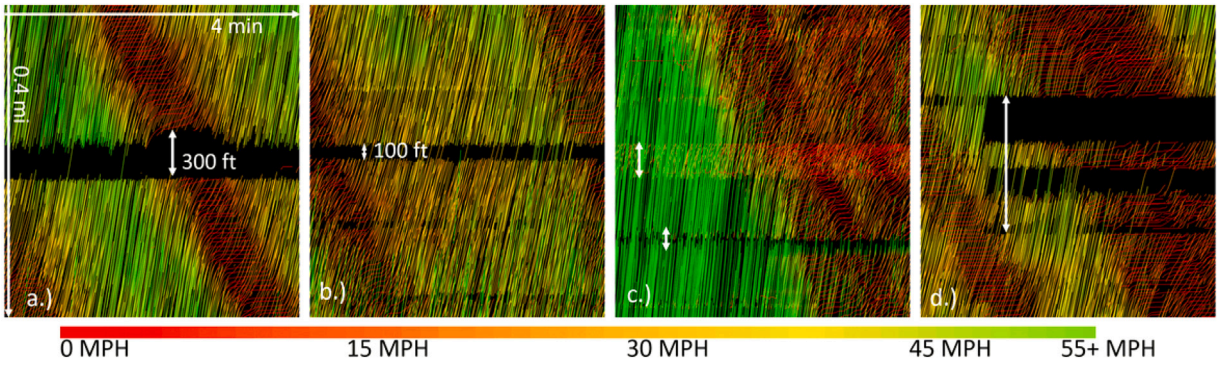

Fig. 10. Example artifacts. For all figures, horizontal scale = 4 min. and vertical scale = 0.4 mi. (a) Missing pole causes a wide band of missing data. (b) Overpass causes a narrow band of missing data. In some cases post-processing can successfully stitch trajectories through this occlusion. (c) Homography error causes multiple trajectories corresponding to the same vehicle, or else results in a narrow band with no coverage. (d) Packet drops cause bands of missing trajectory data with a discrete start and end. Post-processing only partially fills in this data.

- **Packet Drops/Frame Corruptions:** Network bandwidth limitations (especially near night-time hours when low light conditions create noisier and therefore larger video data) result in occasional packet drops or frame corruptions, which manifest as a band of missing positional data for a contiguous region of space and time. This issue will be mostly addressed by IP camera stream profile optimization and network connectivity improvements.
- **Fragmentations:** Ideally, each vehicle passing through the instrument is represented by a single recorded trajectory. In practice though, vehicles are often represented by several trajectory fragments, which are often the product of the above artifacts or other tracking or post-processing failures. Fragmentations manifest as discontinuous chunks of trajectory corresponding to a single vehicle. Fragmentations will be iteratively decreased over time as the above artifacts and other tracking issues are removed.

4.5. Data availability

At the time of publication, data from I-24 MOTION will be made available on the project website located at https://i24motion.org/data. For review purposes, data is available at Gloudemans et al. (2023b). Data will be associated with a DOI for permanent referencing, and new versions of data will be assigned new DOIs according to standard DOI issuing guidelines. A README file contains information relevant to downloading, formatting, and using the data. Each processed day of data (a JSON set of JSON-like trajectories) is made available for download, as well as additional metadata including: scene homography for the data, trajectory extraction algorithm settings, and in-depth descriptions of data attributes. Data is initially released "as is", recognizing over time the data will be reprocessed and improved as the instrument matures. New versions of this dataset will be updated as notable changes occur. Additional datasets (e.g., detailed lane markings) will be documented and released at the project website at https://i24motion.org/data as they become available. Video data is in general not persistently recorded or made available with trajectory data. This is because the raw video data potentially contains *personally identifiable information*. The instrument and data processing was designed to avoid collecting PII but it is difficult to guarantee no information was collected for all but very small subsets of data. We also note that the size of raw video files from the entire instrument is too large for easy distribution. For example the initial data release corresponds to approximately 47TB of video files. Depending on research community needs and IRB considerations, it is possible this may be reconsidered in the future.

5. Discussion

This section provides some initial analysis of the datasets that are released with the publication. We generate the time–space diagrams of all of the published datasets, as well as illustrations of the type of analysis that can be conducted on the current data.

5.1. Traffic wave properties

Traffic oscillations are characterized by regular acceleration/deceleration cycles in congested traffic, and is shown to have negative impact on the overall traffic efficiency and energy consumption (Schönhof and Helbing, 2007; Stern et al., 2018). In this subsection we provide a few examples of macroscopic observations from a dataset captured by the I-24 MOTION system during the morning rush hours of two weekdays (Nov. 21 and Nov. 23, 2022) containing multiple events. The time space diagrams for these days are shown in Fig. 11 including a variety of traffic patterns, such as free-flow, congested and stop-and-go traffic as well as bottlenecks caused by various incidents.

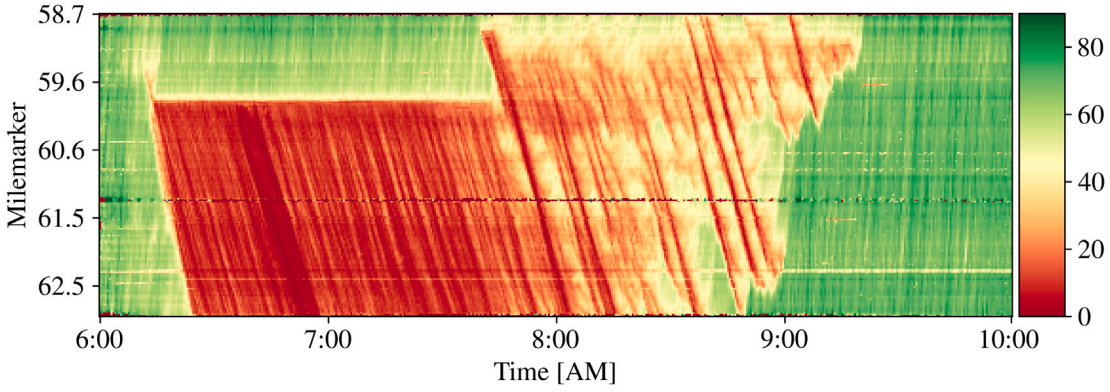

(a) Monday Nov. 21 2022

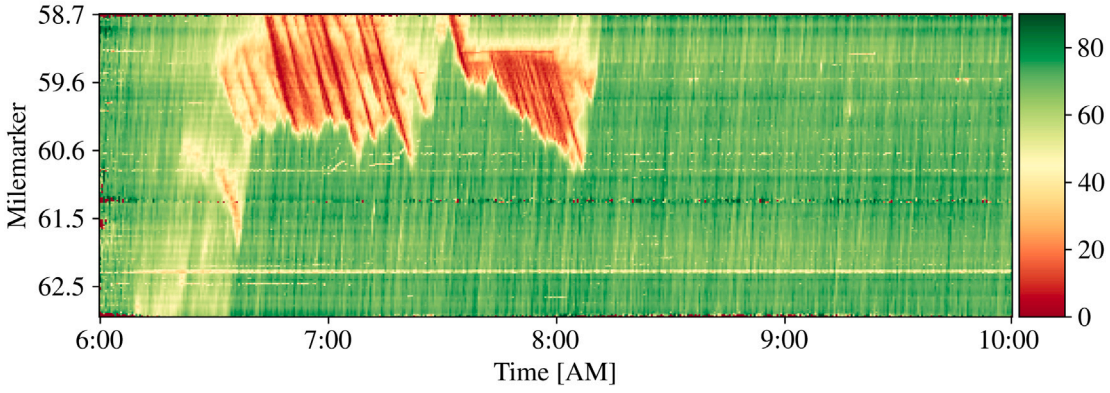

(b) Wednesday Nov. 23 2022

Fig. 11. Velocity field in (mph) obtained from the westbound (decreasing milemarkers) trajectory data on (a) Nov. 21 and (b) Nov. 23, 2022. Each plot depicts traffic velocity evolution during the morning rush hours on the 4-mile of I-24 MOTION main corridor. The velocity field is aggregated into small bins from trajectory data according to Edie's definitions (Edie et al., 1963) with grid size of Δt = 30 s and Δx = 100 ft, respectively. The window sizes are selected to preserve fine-scale traffic wave properties.

Table 7
Approximate traffic wave properties in the upstream segment of selected events. The wave properties are obtained by a combination of wavelet transform and visual inspection (see Appendix E). Almost all waves appear to be "quasi-periodic" and non-stationary and therefore only the most prominent values are reported.

Event information						Upstream wave properties		
Index	Date	Duration	Nearest milemarker	Description	Blocked lanes	Propagation speed (mph)	Period (min)	Fluctuation range (mph)
A	Nov 21	6:14–7:43 AM	MM59.7	Severe rear-end accident	1, 2 and left shoulder	12.6	2.1	0–14.8
B	Nov 21	7:40–7:44 AM	MM58.8	Debris in lane	3	12.5	5.0	8.4–42.5
C	Nov 23	7:35–7:45 AM	MM59.2	Sideswipe accident	1 & 2	13.1	1.8	8.7–19.5

We select three signature events from these days (termed as Events A–C, see Table 7), which are incident-induced bottlenecks. Specifically, Event A is a severe rear-end crash on the HOV lane that was immediately followed by an onset of upstream queuing on lane 1 and lane 2. The congestion lasted for about 1.5 h before the crash was cleared. Event B is a slowdown on lane 3 caused by a large object falling out of a pickup truck. The roadway was cleared about 2.5 min later. Event C is a sideswipe crash due to a

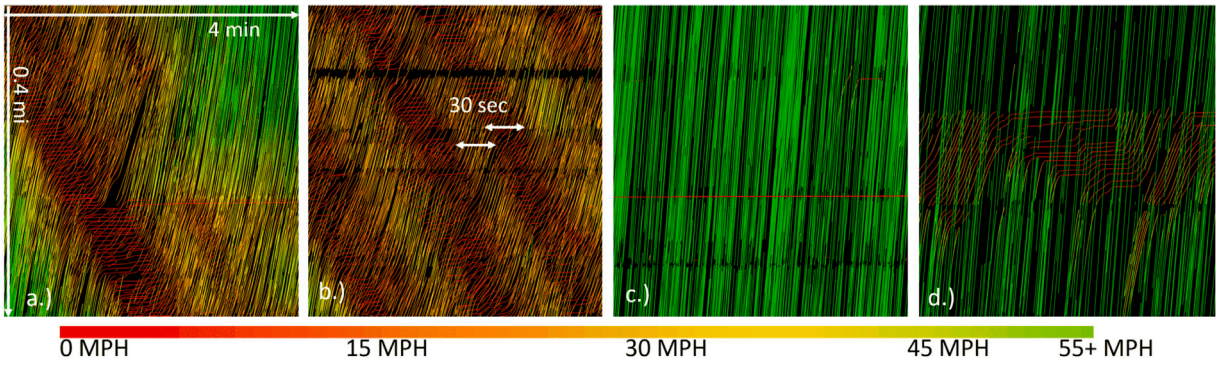

Fig. 12. Examples of data phenomena difficult to observe in fixed-point or sparse GNSS floating vehicle sensing schemes. For all figures, horizontal scale = 4 min and vertical scale = 0.4 mi. (a) Vehicle collision and resulting small-scale bottleneck. (b) Low-wavelength (≈ 30 s) traffic waves in high-density flow. (c) A stopped vehicle on side of roadway. (d) Off-ramp queuing during otherwise free-flow conditions.

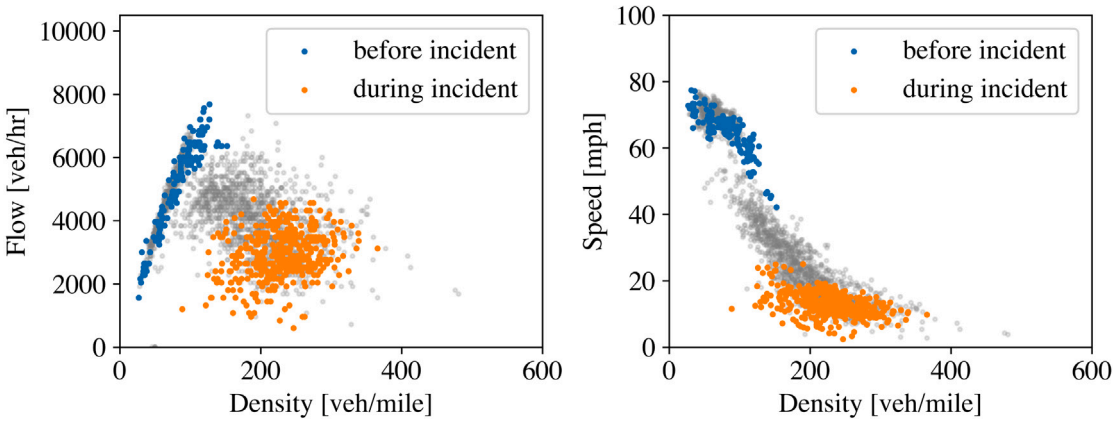

Fig. 13. Flow, density and speed of west bound traffic at MM59.7 before and during event A on Monday Nov 21.

vehicle changing from lane 1 to lane 2 that caused a collision with another car traveling in lane 2. These events are summarized in Table 7.

Characteristics of the waves upstream of the selected events are calculated and also summarized in Table 7, including the wave propagation speed, period (time it takes to experience a complete slowdown and speedup cycle at a fixed location), and amplitude (or fluctuation range). Here the wave property calculations are based on visual inspections combined with various well-known techniques such as wavelet transform (Daubechies, 1992) and cross-correlation (Zielke et al., 2008). We direct interested readers to common references such as Zheng et al. (2011), Zielke et al. (2008) for details.

Fig. 11 shows that perturbations in different times and locations all propagate upstream. Although the periodicity and magnitude of the waves vary, depending on factors such as the severity of the bottleneck, road geometry, and heterogeneity of driver–vehicle units (Zielke et al., 2008), they generally travel against the direction of traffic at a constant characteristic speed of approximately 13 mph (see also Treiber et al. (2010), Helbing et al. (2009), Kerner and Lieu (2005)). We observe that oscillations with longer periods are often accompanied by larger amplitudes. For example, Event A has prominent waves with period 2.1 min and a speed range of 14.8 mph, Event B with period 5 min and a speed range of 34 mph, and Event C with period 1.8 min and a speed range of 10.8 mph, although the severity and the traffic conditions vary. The strong correlation between traffic wave period and amplitude is also discussed in Gartner et al. (2002).

Even in the present form, data from I-24 MOTION already suitable to study traffic waves and other macroscopic quantities. This allows I-24 MOTION data to be used for speed analysis directly without needing to extrapolate long distances between fixed sensors (data cleaning is, however still required). Moreover, the camera-based sensors yield useful insight into the initial causes of

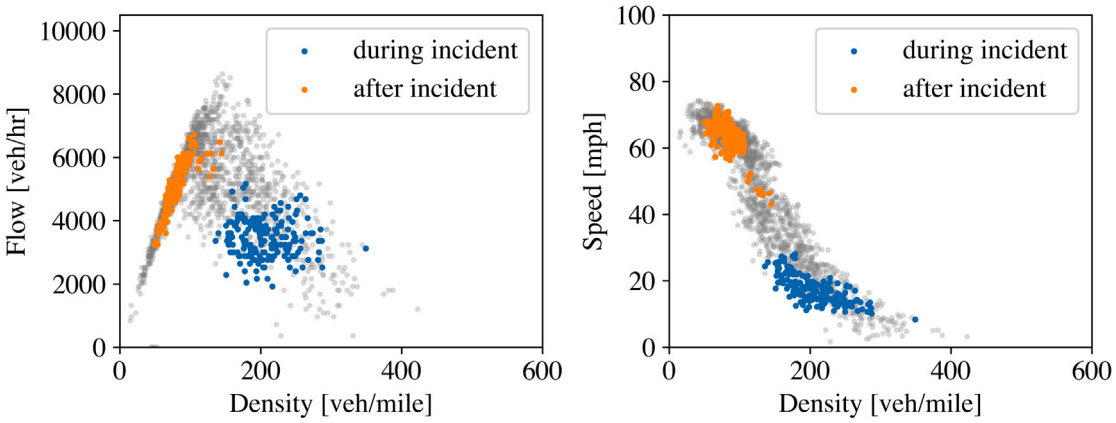

Fig. 14. Flow, density and speed of west bound traffic at MM59.2 during and after event C on Wednesday Nov 23.

bottlenecks not visible in any other sensing modality (e.g., debris on the roadway). Fig. 12 shows other example traffic phenomena not easily visible in traditional traffic sensing regimes.

5.2. Fundamental diagrams (FDs)

The empirical data from I-24 MOTION provides high resolution spatial–temporal evolution of traffic, which allows us to investigate more closely the changes of traffic properties on a finer scale. It also provides the possibility of computing fundamental diagrams at arbitrary locations around incidents.

For example, Figs. 13–14 show the flow, density and speed relationship at approximately 1000 ft upstream of event A and C, respectively, where there is 4 lanes of traffic. Specifically, the gray points in Fig. 13 show all the traffic data at MM 59.7 during the 4-hr recording period from 6:00–10:00 AM; the blue points correspond to the traffic data at the same location from 6:00 AM to 6:15 AM, immediately before the crash event A; the orange points show the most congested 15 min during the incident. Similarly, the blue points in Fig. 14 represent the traffic data from 7:45 AM to 8:00 AM at MM59.2 during event C, the orange color corresponds to a 15-minute interval after the congestion is cleared, and the gray points are all the traffic data at MM59.2. The points are computed from the trajectory data using Edie's definitions. This illustrates a capability that is possible to explore precisely because the complete roadway is monitored, allowing us to analyze the data around each event location.

5.3. Lane level wave analysis

The data from I-24 MOTION allows us to explore how waves propagate lane by lane. In Fig. 15, we show the time space diagrams associated with the traffic conditions recorded on November 30, 2022. The data is shown by lane. Lane 1 is a high occupancy vehicle lane and is furthest from the freeway merges and diverges. Lanes increase in number from left to right where Lane 4 handles all vehicles merging into the freeway or exiting from the freeway. The images are colored on a red-green color-scale to better highlight the wave structure, with red associated with the slow moving traffic and green associated with fast traffic.

Comparing Lane 1 data (Fig. 15(a)) to Lane 4 data (Fig. 15(d)), we see that the waves tend to be disrupted in Lane 4. In Lane 1, waves travel without disruption the full length of the roadway after they are formed. In contrast, waves in Lane 4 are disrupted and reform at multiple locations. As more data is collected, it will be interesting to determine if these patterns are repeated and if the mechanism to explain these patterns can be identified.

The current illustrations provided here are not comprehensive but are rather designed to show that the data in its current form can already be used to support different research questions. As the datasets continue to improve, it will allow further investigations that bridge microscopic and macroscopic scales. It may also allow labeling of vehicle trajectories under level 1 automated vehicle velocity control, for example using unsupervised methods (Khajeh Hosseini et al., 2022). Many of the best selling vehicles in the US have adaptive cruise control as a standard or optional feature now for several years, and consequently they are likely already in the datasets contained in this work. Labeling these vehicles could further aid understanding of the interactions between automated vehicles and human piloted ones.

6. Conclusion

This work introduces the I-24 MOTION instrument, which is designed to produce large scale trajectory datasets to support new directions in traffic science and traffic flow theory research. We also provide our initial datasets that will be improved and maintained as the instrument software continues to mature.

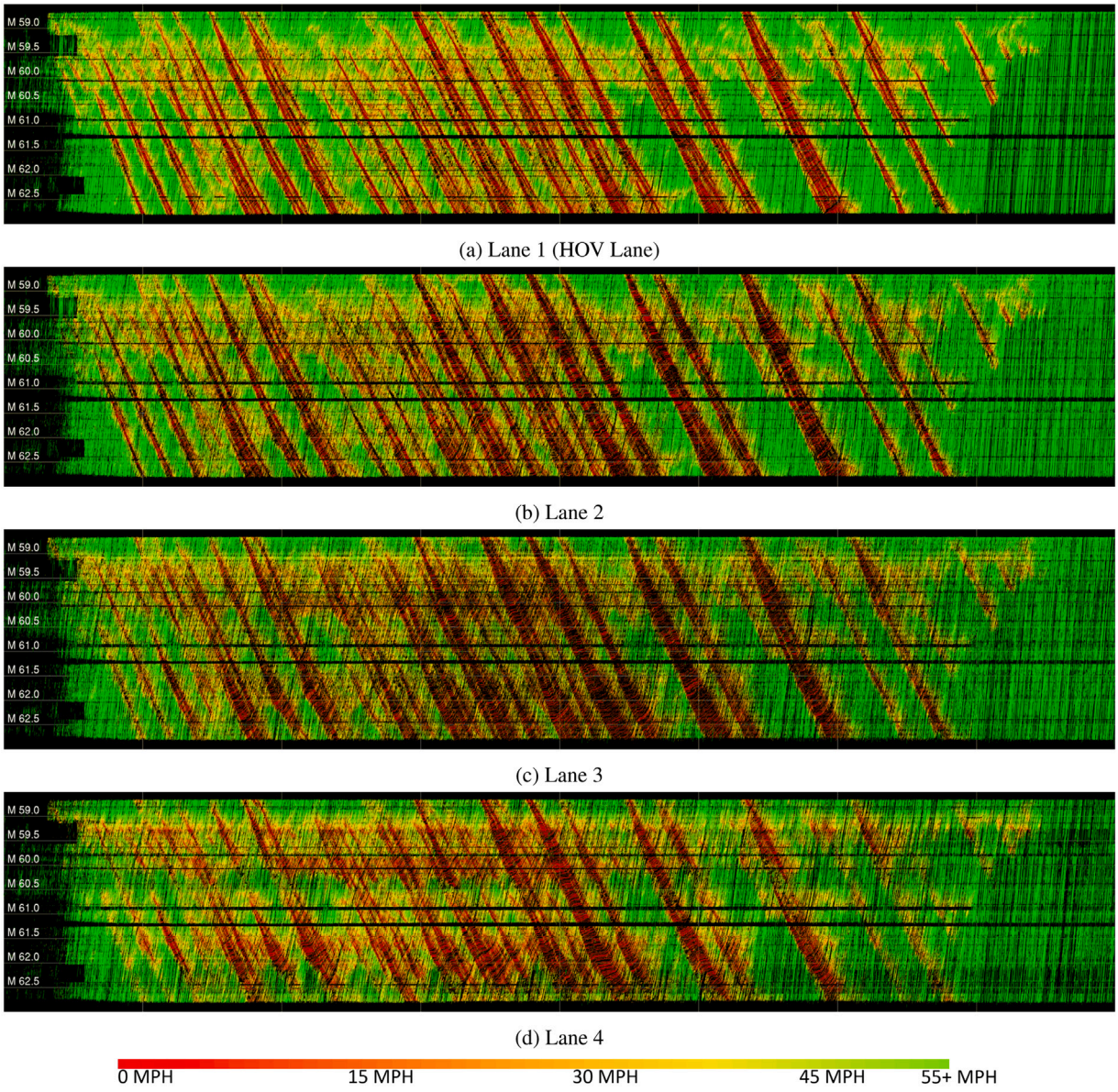

Fig. 15. Wednesday, Nov 30 2022, 6:00–10:00 AM traffic waves by lane visible in time space diagrams. Figure (a) Lane 1 (High Occupancy Vehicle lane); (b) Lane 2; (c) Lane 3; (d) Lane 4 (closest to entrance and exit ramps). Traffic speeds are shaded green (fastest) to red (slowest). Lane positions are roughly approximated as constant lateral ranges, estimated by averaging the lateral coordinates of all lane markings for each lane. Comparing the waves in Lane 1 (a) to Lane 4 (d), the waves appear to travel the further and without interruption in Lane 1.

Physical infrastructure construction on the instrument completed in November 2022, and the processing algorithms are far from final. In our ongoing work, we will be providing more datasets, tools, and methods, and software implementations that allow the instrument to support a wider range of applications and increase the overall data quality, using as inspiration similar developments on the pNEUMA dataset (Kim et al., 2023). Recognizing the evolving nature of the instrument, this work serves as a single reference to I-24 MOTION, with future works outlining the methodological improvements that advance data quality and provide insights into the traffic phenomena captured by the instrument.

The instrument was also designed to support live experiments in traffic, including large deployments of automated vehicles which are designed to smooth traffic jams. The instrument will also support experiments conducted in collaboration with Tennessee Department of Transportation to support active traffic management, including experiments using variable speed limits, ramp meters, and lane closure systems. Such experiments will allow further investigation of the consequences of emerging technologies on traffic flow.

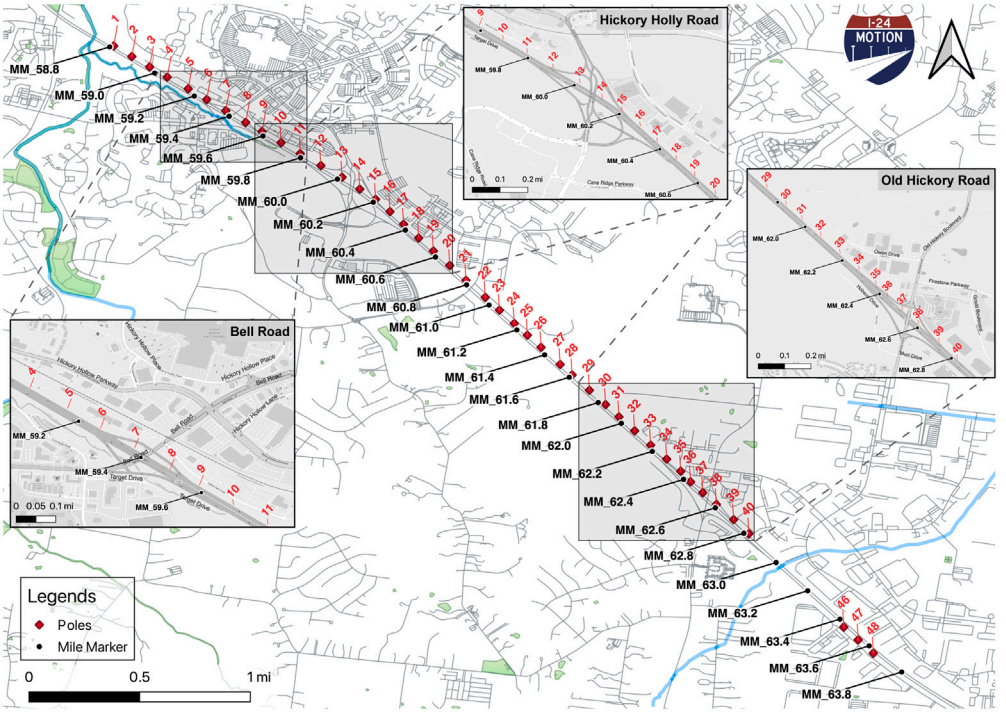

Fig. 16. Map for I-24 MOTION infrastructure locations.

Table 8
I-24 MOTION mile markers locations.

Mile marker	Point ID	Longitude	Latitude	State plane X	State plane Y
58.8	MM_58.8	−86.66866410	36.05094709	1770838.696	625898.5077
59.0	MM_59.0	−86.66503515	36.04884254	1771906.217	625125.1057
59.2	MM_59.2	−86.66183360	36.04698293	1772848.051	624441.7616
59.4	MM_59.4	−86.65902194	36.04535112	1773675.225	623842.1457
59.6	MM_59.6	−86.65629355	36.04376336	1774477.926	623258.7510
59.8	MM_59.8	−86.65326486	36.04200469	1775369.021	622612.5765
60.0	MM_60.0	−86.65028677	36.04027637	1776245.271	621977.5736
60.2	MM_60.2	−86.64739949	36.03842164	1777094.407	621296.7643
60.4	MM_60.4	−86.64480563	36.03616949	1777855.880	620471.8813
60.6	MM_60.6	−86.64237969	36.03399726	1778567.938	619676.4352
60.8	MM_60.8	−86.63987316	36.03175206	1779303.690	618854.2919
61.0	MM_61.0	−86.63805753	36.03012361	1779836.660	618258.0070
61.2	MM_61.2	−86.63581527	36.02811365	1780494.901	617522.0338
61.4	MM_61.4	−86.63357648	36.02609495	1781152.126	616782.9034
61.6	MM_61.6	−86.63159535	36.02429507	1781733.708	616123.9322
61.8	MM_61.8	−86.62925595	36.02224969	1782420.689	615374.9230
62.0	MM_62.0	−86.62739188	36.02057890	1782968.012	614763.1915
62.2	MM_62.2	−86.62489214	36.01831143	1783701.957	613933.0703
62.4	MM_62.4	−86.62236859	36.01605276	1784443.006	613106.1225
62.6	MM_62.6	−86.61980346	36.01376075	1785196.314	612266.9811
62.8	MM_62.8	−86.61751107	36.01170527	1785869.549	611514.4733
63.0	MM_63.0	−86.61490413	36.00934448	1786635.150	610650.2540
63.4	MM_63.4	−86.60975712	36.00477456	1788147.059	608977.2122
63.2	MM_63.2	−86.61235700	36.00705984	1787383.284	609813.8888
63.6	MM_63.6	−86.60739940	36.00261699	1788839.540	608187.4889
63.8	MM_63.8	−86.60477555	36.00051307	1789610.898	607416.8232

CRediT authorship contribution statement

Derek Gloudemans: Conceptualization, Data curation, Methodology, Software, Visualization, Writing. **Yanbing Wang:** Formal analysis, Investigation, Methodology, Software, Writing. **Junyi Ji:** Data curation, Investigation, Methodology, Validation, Visualization. **Gergely Zachár:** Conceptualization, Investigation, Software, Visualization. **William Barbour:** Conceptualization, Investigation, Software, Writing. **Eric Hall:** Resources, Software. **Meredith Cebelak:** Conceptualization, Funding acquisition, Resources. **Lee Smith:** Conceptualization, Funding acquisition, Resources. **Daniel B. Work:** Conceptualization, Funding acquisition, Project administration, Resources, Writing.

Data availability

Link to data for review purposes is included in the manuscript.

Acknowledgments

The authors would like to thank Brad Freeze, Mohamed Osman, Michelle Nickerson the Tennessee Department of Transportation, Matt D'Angelo and Gresham Smith for their efforts on conceptualizing, designing, and implementing the system, Craig Philip and Janos Sztipanovits for their assistance conceptualizing I-24 MOTION. The authors would like to thank Zi Nean Teoh and Lisa Liu for their contributions to develop, build and deploy the I-24 MOTION software. The authors are grateful to Davis H. Elliot for constructing the instrument, MG-Squared for designing and manufacturing the camera mounting bracket and lowering device, and WSP for serving as CEI for I-24 MOTION construction. This work is supported by the National Science Foundation (NSF), United States under Grant No. 2135579, the NSF Graduate Research Fellowship Grant No. DGE-1937963 and the USDOT Dwight D. Eisenhower Fellowship program, United States under Grant No. 693JJ32245006 (Gloudemans) and No. 693JJ322NF5201 (Wang). This material is based upon work supported by the U.S. Department of Energy's Office of Energy Efficiency and Renewable Energy (EERE) award number CID DE-EE0008872. This material is based upon work supported by the CMAQ award number TN20210003. The views expressed herein do not necessarily represent the views of the Tennessee Department of Transportation, U.S. Department of Energy, or the United States Government.

Appendix A. I-24 motion infrastructure locations

See Fig. 16, Tables 8 and 9.

Appendix B. Example vehicle trajectory

See Tables 10 and 11.

Appendix C. Additional time space diagrams

See Fig. 17.

Appendix D. Platoon consistency

Platoon consistency refers to the physical consistency of inter-vehicle spacing resulting from the individual trajectories of two following vehicles (Montanino and Punzo, 2015). The leader–follower pair and their longitudinal gap are calculate at each timestamp. Fig. 18 shows a histogram of the inter-vehicle gaps distribution from the 4-hr westbound traffic data captured on November 21, 2022 as an example. Note that a small portion of the gaps are negative, and this is due to the artifacts mentioned above including (a) homography error that causes multiple trajectories corresponding to the same vehicle, and (2) current data association step fails to connect partially overlapped trajectories of the same vehicle, creating the appearance of 2 vehicles when in fact there is a single vehicle. These artifacts cause overlaps in trajectories which may not accurately reflect the platoon consistency. Addressing these issues with more robust homography estimation and data association techniques is an on-going effort, and we expect many of these artifacts to be reduced in the next release.

Appendix E. Traffic wave calculations

E.1. Wave propagation speed

The wave propagation speed is characterized by the slope of the slowdown that propagates upstream in the time–space diagram shown in 11. The slope is calculated based on the cross-correlation method as used in Coifman and Wang (2005), Zielke et al. (2008), which compares the time series of the speed signals observed at two nearby locations on the same congested freeway. The idea is to shift one signal relative to another until the first non-trivial peaks are matched. The wave propagation speed is therefore the ratio between the time shifted and the distance of these two locations. We randomly select a few pairs of locations from one trajectory dataset and obtain a distribution of propagation speed. The distribution for the morning of Nov 22 2022, for example, has a mean of 12.8 mph and a standard deviation of 0.5 mph.

Table 9
I-24 MOTION camera poles locations.

Pole number	Longitude	Latitude	State plane X	State plane Y
1	−86.66833967	36.05102465	1770934.792	625926.0873
2	−86.66687250	36.05017024	1771366.371	625612.1079
3	−86.66544020	36.04933317	1771787.694	625304.5168
4	−86.66401863	36.04851127	1772205.892	625002.4762
5	−86.66233152	36.04756791	1772702.297	624655.6994
6	−86.66083753	36.04669178	1773141.790	624333.7851
7	−86.65929794	36.04579394	1773594.718	624003.8887
8	−86.65769130	36.04484839	1774067.364	623656.4946
9	−86.65637702	36.04412186	1774454.125	623389.4189
10	−86.65484011	36.04321966	1774906.280	623057.9590
11	−86.65329516	36.04233914	1775360.877	622734.3812
12	−86.65162683	36.04137402	1775851.755	622379.7744
13	−86.64991826	36.04043058	1776354.592	622032.9875
14	−86.64848596	36.03947629	1776775.738	621682.7990
15	−86.64721191	36.03865212	1777150.421	621380.2927
16	−86.64605051	36.03766310	1777491.410	621018.0047
17	−86.64495349	36.03663936	1777813.291	620643.2092
18	−86.64373577	36.03553102	1778170.665	620237.3857
19	−86.64255023	36.03448123	1778518.672	619852.9414
20	−86.64123058	36.03331430	1778906.061	619425.6000
21	−86.63992435	36.03211698	1779289.424	618987.2296
22	−86.63836598	36.03073961	1779746.919	618482.8354
23	−86.63722336	36.02970928	1780082.325	618105.5763
24	−86.63602978	36.02863772	1780432.712	617713.2157
25	−86.63496763	36.02768979	1780744.537	617366.1146
26	−86.63386524	36.02670063	1781068.170	617003.9328
27	−86.63232565	36.02533401	1781520.201	616503.5170
28	−86.63136274	36.02448366	1781802.936	616192.1370
29	−86.62996531	36.02324282	1782213.251	615737.7900
30	−86.62866175	36.02208874	1782596.022	615315.2072
31	−86.62758082	36.02109301	1782913.340	614950.6926
32	−86.62631750	36.01997360	1783284.314	614540.8191
33	−86.62502736	36.01881730	1783663.145	614117.4689
34	−86.62373185	36.01768485	1784043.629	613702.7945
35	−86.62259996	36.01670424	1784376.089	613343.7080
36	−86.62180603	36.01586031	1784608.928	613035.0094
37	−86.62081629	36.01498165	1784899.597	612713.3060
38	−86.61972731	36.01402487	1785219.443	612362.9850
39	−86.61833256	36.01280557	1785629.123	611916.5303
40	−86.61710143	36.01166435	1785990.606	611498.8117
46	−86.60944641	36.00413537	1788237.510	608743.9647
47	−86.60828501	36.00309818	1788578.679	608364.2754
48	−86.60706192	36.00202409	1788938.020	607971.0443

Table 10
Detailed information of the example trajectory.

Attribute	Type	Unit	Value
_id	12-byte BSON	–	63732b74e1fa5a45ae0c2fdd
Vehicle class	int	–	0
First timestamp	float	s	1668436223.30
Last timestamp	float	s	1668436257.60
Timestamp	[float]	s	See Table 11
x position	[float]	ft	See Table 11
y position	[float]	ft	See Table 11
Starting x	float	ft	325400.5531
Ending x	float	ft	329300.5458
Length	float	ft	15.6381
Width	float	ft	5.8521
Height	float	ft	4.7021
Direction	int	–	1
Configuration ID	int	–	−1

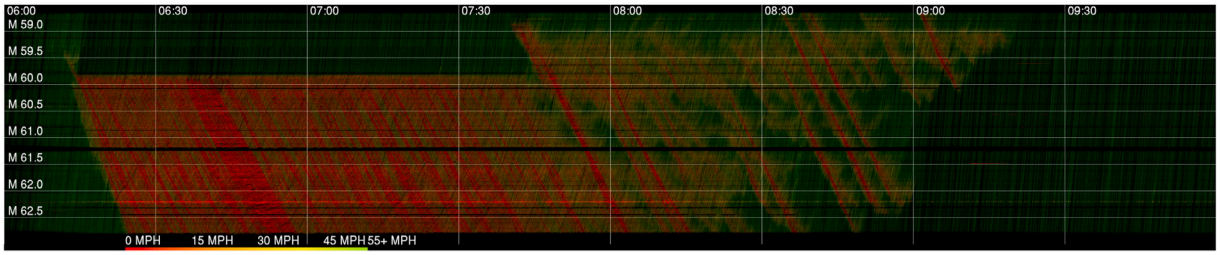

(a) Monday Nov 21 2022

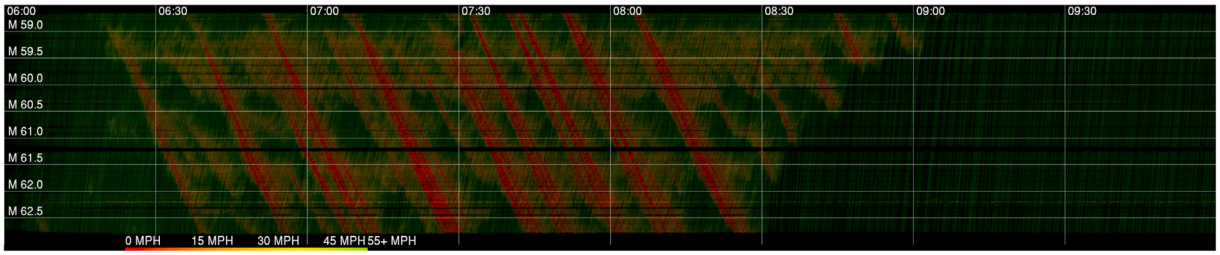

(b) Tuesday Nov 22 2022

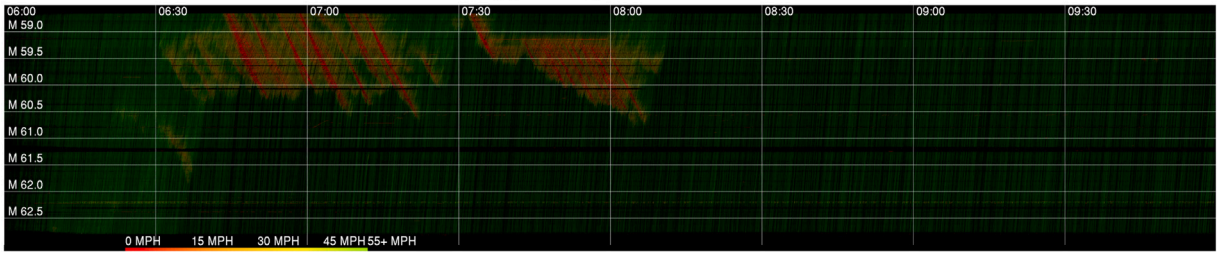

(c) Wednesday Nov 23 2022

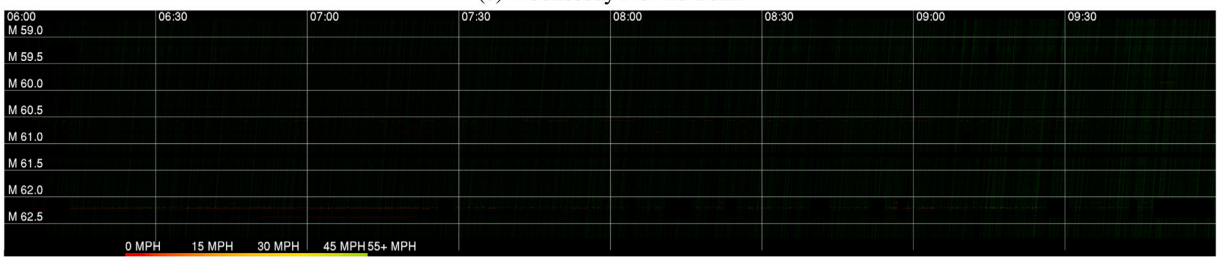

(d) Thursday Nov 24 2022 (Thanksgiving)

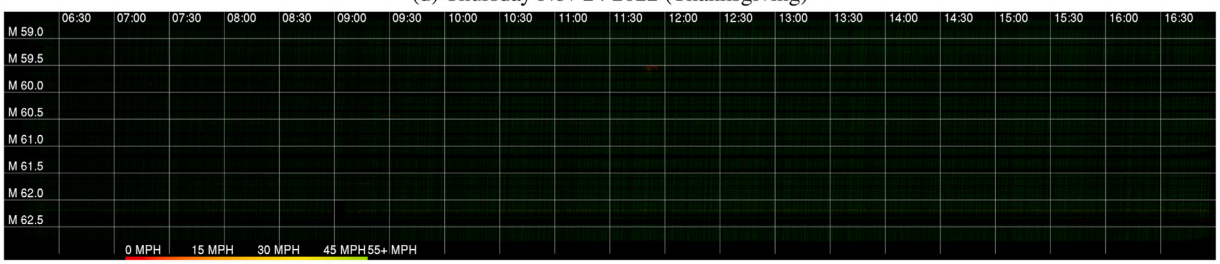

(e) Friday Nov 25 2022 (Black Friday)

Fig. 17. Additional time–space diagrams for I-24 westbound during morning rush hours on (a) Nov 21, (b) Nov 23, (c) Nov 29, (d) Dec 1 and (e) Dec 2, 2022.

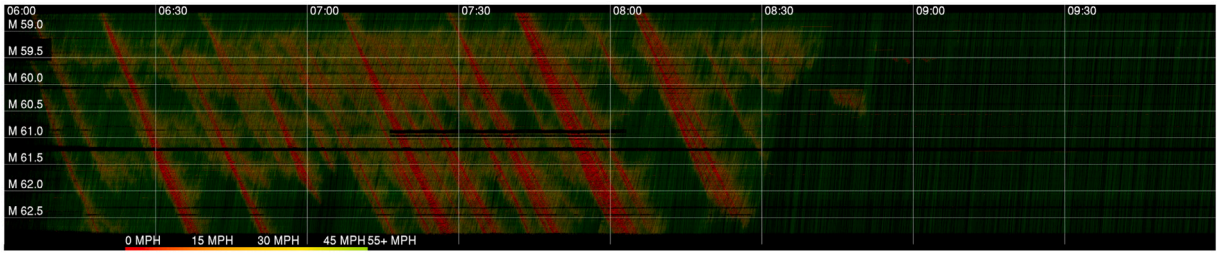

(f) Monday Nov 28 2022

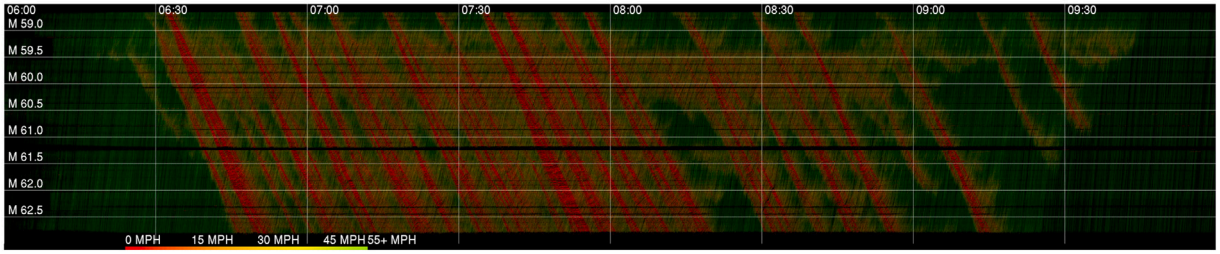

(g) Tuesday Nov 29 2022

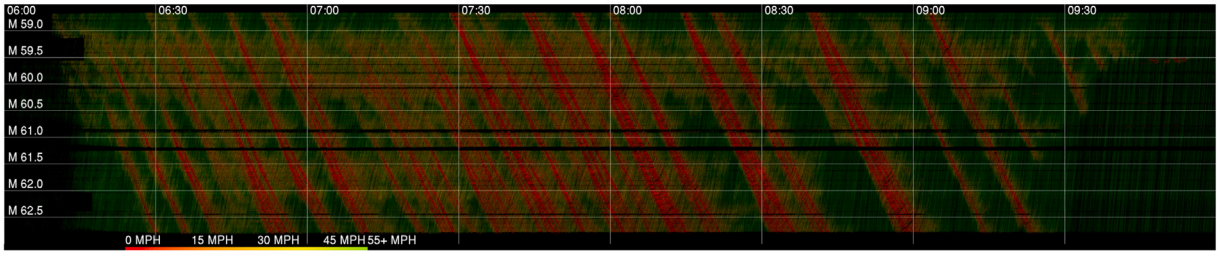

(h) Wednesday Nov 30 2022

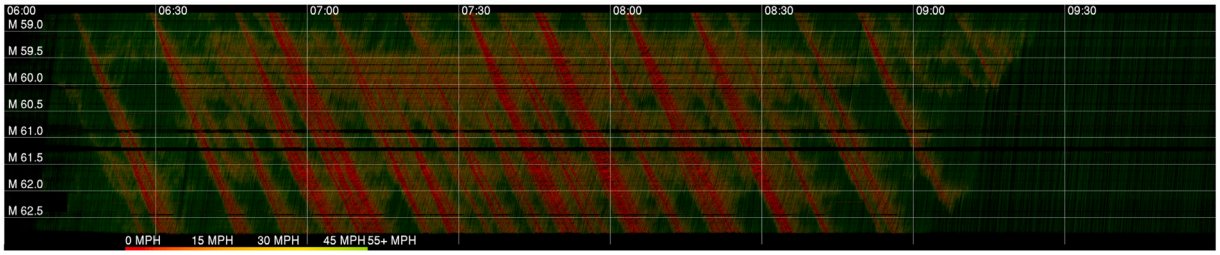

(i) Thursday Dec 1 2022

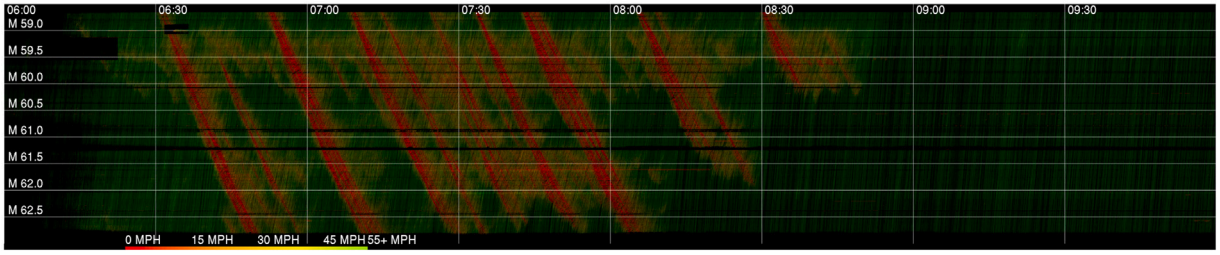

(j) Friday Dec 2 2022

Fig. 17. (*continued*).

E.2. Wave frequency analysis

Wavelet transform is a time–frequency decomposition tool to effectively extract the non-stationary wave properties present in signals. The continuous wavelet transform is a convolution of the time-series signal $x(t)$ with a set of functions generated by the

Table 11
The first 5 and the last 5 trajectory points for the example trajectory.

Timestamp (s)	x position (ft)	y position (ft)
1668436223.30	325400.5531	−19.19265508
1668436223.34	325405.0238	−19.12047988
1668436223.38	325409.4943	−19.04921183
1668436223.42	325413.9646	−18.97885093
1668436223.46	325418.4349	−18.90939717
...	...	...
1668436257.42	329281.8317	−43.03453987
1668436257.46	329286.5097	−43.09132499
1668436257.50	329291.1881	−43.14893520
1668436257.54	329295.8668	−43.20737050
1668436257.58	329300.5458	−43.26663087

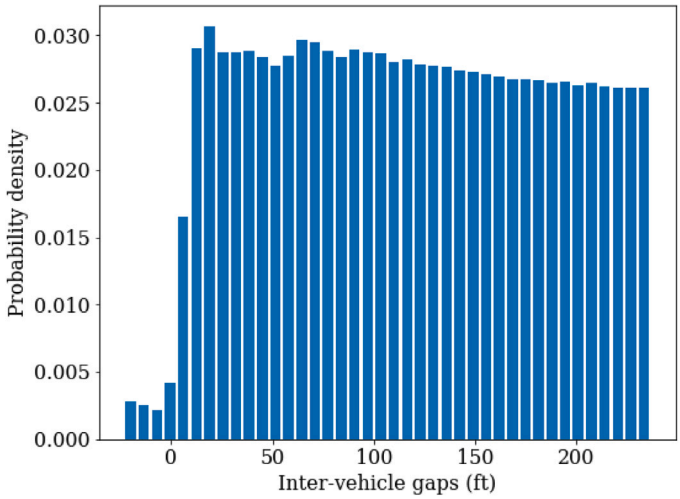

Fig. 18. Distribution of inter-vehicle gaps for westbound traffic during 6:00–10:00 AM on Monday, November 21, 2022.

mother wavelet $\psi(t)$:

$$X_w(a,b) = \frac{1}{|a|^{1/2}} \int_{-\infty}^{\infty} x(t)\psi\left(\frac{t-b}{a}\right) dt, \tag{1}$$

where $X_w(a,b)$ is a transformed signal at location b and scale a in the wavelet dimension. The scaling factor and the translation factor vary continuously, providing an overcomplete representation of the signals. We select a commonly used mother wavelet as a Morlet wavelet:

$$\psi(t) = e^{-\frac{t^2}{2}} \cos(5t). \tag{2}$$

An example of wavelet transform result is shown in Fig. 19. The top figure shows the time-series of speed sampled at a fixed location (in this case MM61.2) on Tuesday, Nov 29 2022. The bottom one is the corresponding wavelet transform scaleogram of the signal. It is obvious that the traffic waves do not appear to be stationary, i.e., the speed oscillation does not have a unique and consistent frequency across time. For example, during 6:50 AM–7:30 AM, the power of the signal peaks around 6.7 min, corresponding to a salient wave period of 6.7 min; during 8:30 AM–9:30 AM, the prominent wave period is near 9 min.

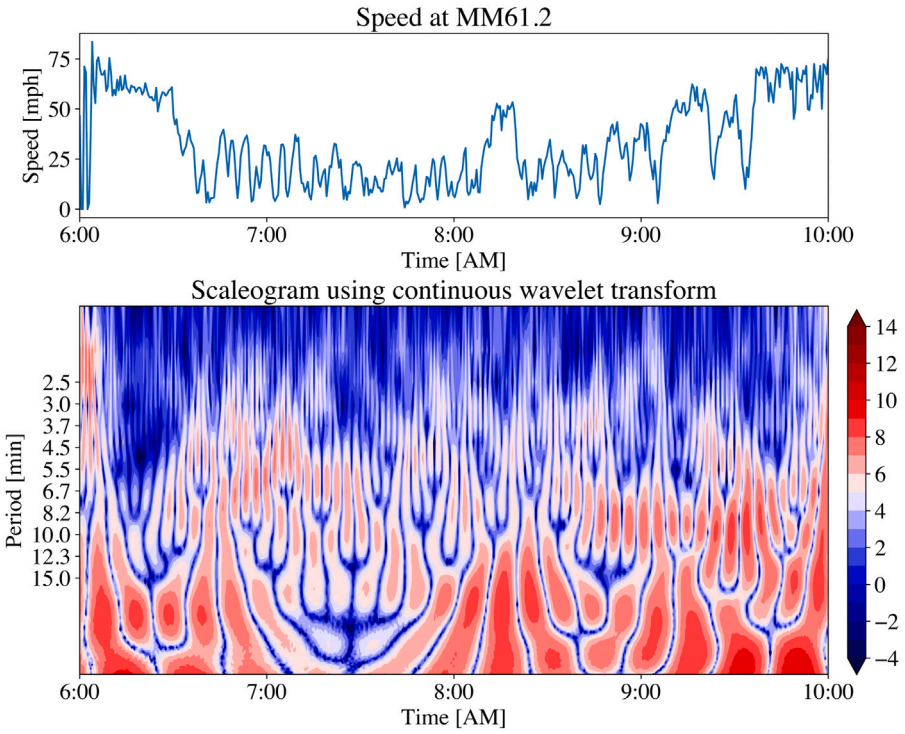

Fig. 19. Top: The speed time-series sampled from MM61.2 on Tuesday, Nov 29 2022. Bottom: A scaleogram produced by continuous wavelet transform of the speed signal. The color represents log-scale of the power distribution across both frequency and time domain of the signal.

References

Alexiadis, V., Colyar, J., Halkias, J., Hranac, R., McHale, G., 2004. The next generation simulation program. Inst. Transp. Eng. ITE J. 74 (8), 22.

Altché, F., de La Fortelle, A., 2017. An LSTM network for highway trajectory prediction. In: 2017 IEEE 20th International Conference on Intelligent Transportation Systems. ITSC, IEEE, pp. 353–359.

Ambarwati, L., Pel, A.J., Verhaeghe, R., van Arem, B., 2014. Empirical analysis of heterogeneous traffic flow and calibration of porous flow model. Transp. Res. C 48, 418–436.

American Center for Mobility, 2021. Mobility research. https://www.acmwillowrun.org/. (Online accessed April 2021).

Arasan, V.T., Koshy, R.Z., 2005. Methodology for modeling highly heterogeneous traffic flow. J. Transp. Eng. 131 (7), 544–551.

Aw, A., Rascle, M., 2000. Resurrection of" second order" models of traffic flow. SIAM J. Appl. Math. 60 (3), 916–938.

Bahari, M., Nejjar, I., Alahi, A., 2021. Injecting knowledge in data-driven vehicle trajectory predictors. Transp. Res. C 128, 103010.

Bar-Gera, H., 2007. Evaluation of a cellular phone-based system for measurements of traffic speeds and travel times: A case study from Israel. Transp. Res. C 15 (6), 380–391.

Barbour, W., Gloudemans, D., Cebelak, M., Freeze, P.B., Work, D.B., 2020. Interstate 24 motion open road testbed. URL https://i24motion. org.

Barmpounakis, E., Geroliminis, N., 2020. On the new era of urban traffic monitoring with massive drone data: The pNEUMA large-scale field experiment. Transp. Res. C 111, 50–71.

Berclaz, J., Fleuret, F., Fua, P., 2009. Multiple object tracking using flow linear programming. In: 2009 Twelfth IEEE International Workshop on Performance Evaluation of Tracking and Surveillance. IEEE, pp. 1–8.

Bernardin, K., Stiefelhagen, R., 2008. Evaluating multiple object tracking performance: the CLEAR MOT metrics. EURASIP J. Image Video Process. 2008, 1–10.

Bochinski, E., Eiselein, V., Sikora, T., 2017. High-speed tracking-by-detection without using image information. In: 2017 14th IEEE International Conference on Advanced Video and Signal Based Surveillance. AVSS, IEEE, pp. 1–6.

Bock, J., Krajewski, R., Moers, T., Runde, S., Vater, L., Eckstein, L., 2020. The inD dataset: A drone dataset of naturalistic road user trajectories at german intersections. In: 2020 IEEE Intelligent Vehicles Symposium. IV, pp. 1929–1934.

Breuer, A., Termöhlen, J.-A., Homoceanu, S., Fingscheidt, T., 2020. openDD: A large-scale roundabout drone dataset. In: 2020 IEEE 23rd International Conference on Intelligent Transportation Systems. ITSC, IEEE, pp. 1–6.

Briefs, U., 2015. Mcity grand opening. Res. Rev. 46 (3).

Bunting, M., Bhadani, R., Sprinkle, J., 2021. Libpanda: a high performance library for vehicle data collection. In: Proceedings of the Workshop on Data-Driven and Intelligent Cyber-Physical Systems. In: DI-CPS'21, Association for Computing Machinery, New York, NY, USA, ISBN: 9781450384452, pp. 32–40.

Chandler, R.E., Herman, R., Montroll, E.W., 1958. Traffic dynamics: studies in car following. Oper. Res. 6 (2), 165–184.

Chen, D., Ahn, S., 2015. Variable speed limit control for severe non-recurrent freeway bottlenecks. Transp. Res. C 51, 210–230.

Chen, Y., Jing, L., Vahdani, E., Zhang, L., He, M., Tian, Y., 2019. Multi-camera vehicle tracking and re-identification on AI city challenge 2019. In: CVPR Workshops, Vol. 2. pp. 324–332.

Choe, T., Skabardonis, A., Varaiya, P., 2002. Freeway performance measurement system: operational analysis tool. Transp. Res. Rec. 1811 (1), 67–75.

Coifman, B., Li, L., 2017. A critical evaluation of the Next Generation Simulation (NGSIM) vehicle trajectory dataset. Transp. Res. B 105, 362–377.

Coifman, B.A., Wang, Y., 2005. Average velocity of waves propagating through congested freeway traffic. In: Transportation and Traffic Theory. Flow, Dynamics and Human Interaction. 16th International Symposium on Transportation and Traffic TheoryUniversity of Maryland. College Park.

Cosgun, A., Ma, L., Chiu, J., Huang, J., Demir, M., Anon, A.M., Lian, T., Tafish, H., Al-Stouhi, S., 2017. Towards full automated drive in urban environments: A demonstration in gomentum station, california. In: 2017 IEEE Intelligent Vehicles Symposium. IV, IEEE, pp. 1811–1818.
Daubechies, I., 1992. Ten Lectures on Wavelets. SIAM.
Deng, J., Dong, W., Socher, R., Li, L.-J., Li, K., Fei-Fei, L., 2009. Imagenet: A large-scale hierarchical image database. In: 2009 IEEE Conference on Computer Vision and Pattern Recognition. IEEE, pp. 248–255.
Deo, N., Trivedi, M.M., 2018. Multi-modal trajectory prediction of surrounding vehicles with maneuver based lstms. In: 2018 IEEE Intelligent Vehicles Symposium. IV, IEEE, pp. 1179–1184.
Duan, K., Bai, S., Xie, L., Qi, H., Huang, Q., Tian, Q., 2019. Centernet: Keypoint triplets for object detection. In: Proceedings of the IEEE/CVF International Conference on Computer Vision. pp. 6569–6578.
Dubská, M., Herout, A., Juránek, R., Sochor, J., 2014a. Fully automatic roadside camera calibration for traffic surveillance. IEEE Trans. Intell. Transp. Syst. 16, 1162–1171.
Dubská, M., Herout, A., Sochor, J., 2014b. Automatic camera calibration for traffic understanding.. In: BMVC, Vol. 4. p. 8.
Edie, L.C., et al., 1963. Discussion of Traffic Stream Measurements and Definitions. Port of New York Authority New York.
Emami, A., Sarvi, M., Asadi Bagloee, S., 2020. A review of the critical elements and development of real-world connected vehicle testbeds around the world. Transp. Lett. 1–26.
Farrell, J., Barth, M.J., et al., 2015. Precision Mapping of the California Connected Vehicle Testbed Corridor. Technical Report, California. Dept. of Transportation.
FHWA, 2022. West central alabama ACTION. https://ops.fhwa.dot.gov/fastact/atcmtd/2017/applications/univalabama/project.htm.
Gartner, N.H., Messer, C.J., Rathi, A., 2002. Traffic flow theory-A state-of-the-art report: revised monograph on traffic flow theory. Transp. Res. Int. Documentation.
Girshick, R., 2015. Fast r-cnn. In: Proceedings of the IEEE International Conference on Computer Vision. pp. 1440–1448.
Gloudemans, D., Barbour, W., Gloudemans, N., Neuendorf, M., Freeze, B., ElSaid, S., Work, D.B., 2020. Interstate-24 motion: Closing the loop on smart mobility. In: 2020 IEEE Workshop on Design Automation for CPS and IoT. DESTION, IEEE, pp. 49–55.
Gloudemans, D., Gumm, G., Wang, Y., Barbour, W., Work, D.B., 2023a. The Interstate-24 3D Dataset: a new benchmark for 3D multi-camera vehicle tracking. arXiv preprint arXiv:2308.14833.
Gloudemans, D., Wang, Y., Ji, J., Zachar, G., Barbour, W., Work, D.B., 2023b. I-24 motion trajectory dataset: Review release.
Gloudemans, D., Work, D.B., 2021. Vehicle tracking with crop-based detection. In: 2021 20th IEEE International Conference on Machine Learning and Applications. ICMLA, IEEE, pp. 312–319.
Göhring, D., Wang, M., Schnürmacher, M., Ganjineh, T., 2011. Radar/lidar sensor fusion for car-following on highways. In: The 5th International Conference on Automation, Robotics and Applications. IEEE, pp. 407–412.
Greenberg, H., 1959. An analysis of traffic flow. Oper. Res. 7 (1), 79–85.
Greenshields, B., Bibbins, J., Channing, W., Miller, H., 1935. A study of traffic capacity. In: Highway Research Board Proceedings, Vol. 1935. National Research Council (USA), Highway Research Board.
Gurusinghe, G.S., Nakatsuji, T., Azuta, Y., Ranjitkar, P., Tanaboriboon, Y., 2002. Multiple car-following data with real-time kinematic global positioning system. Transp. Res. Rec. 1802 (1), 166–180.
He, K., Gkioxari, G., Dollár, P., Girshick, R., 2017. Mask r-cnn. In: Proceedings of the IEEE International Conference on Computer Vision. pp. 2961–2969.
He, K., Zhang, X., Ren, S., Sun, J., 2016. Deep residual learning for image recognition. In: Proceedings of the IEEE Conference on Computer Vision and Pattern Recognition. pp. 770–778.
Heery, Sr., F., et al., 2017. The florida connected and automated vehicle initiative: a focus on deployment. Inst. Transp. Eng. ITE J. 87 (10), 33–41.
Helbing, D., 1997. Empirical traffic data and their implications for traffic modeling. Phys. Rev. E 55 (1), R25.
Helbing, D., Treiber, M., 1998. Jams, waves, and clusters. Science 282 (5396), 2001–2003.
Helbing, D., Treiber, M., Kesting, A., Schönhof, M., 2009. Theoretical vs. Empirical classification and prediction of congested traffic states. Eur. Phys. J. B.
Herrera, J.C., Work, D.B., Herring, R., Ban, X.J., Jacobson, Q., Bayen, A.M., 2010. Evaluation of traffic data obtained via GPS-enabled mobile phones: The mobile century field experiment. Transp. Res. C 18 (4), 568–583.
James, R., 2023. Third generation simulation: A closer look at the impact of automated driving systems on traffic.
Jones, W.D., 2001. Keeping cars from crashing. IEEE Spectr. 38 (9), 40–45.
Kerner, B.S., 1999. The physics of traffic. Phys. World 12 (8), 25.
Kerner, B.S., Lieu, H., 2005. The physics of traffic: Empirical freeway pattern features, engineering applications; and theory. Phys. Today 58 (11), 54–56.
Kesting, A., Treiber, M., 2008. Calibrating car-following models by using trajectory data: Methodological study. Transp. Res. Rec. 2088 (1), 148–156.
Khajeh Hosseini, M., Talebpour, A., Devunuri, S., Hamdar, S.H., 2022. An unsupervised learning framework for detecting adaptive cruise control operated vehicles in a vehicle trajectory data. Expert Syst. Appl. 208, 118060.
Khan, S.I., Maini, P., 1999. Modeling heterogeneous traffic flow. Transp. Res. Rec. 1678 (1), 234–241.
Kim, S., Anagnostopoulos, G., Barmpounakis, E., Geroliminis, N., 2023. Visual extensions and anomaly detection in the pNEUMA experiment with a swarm of drones. Transp. Res. C 147, 103966.
Koutsopoulos, H.N., Farah, H., 2012. Latent class model for car following behavior. Transp. Res. B 46 (5), 563–578.
Krajewski, R., Bock, J., Kloeker, L., Eckstein, L., 2018. The highd dataset: A drone dataset of naturalistic vehicle trajectories on german highways for validation of highly automated driving systems. In: 2018 21st International Conference on Intelligent Transportation Systems. ITSC, IEEE, pp. 2118–2125.
Krajewski, R., Moers, T., Bock, J., Vater, L., Eckstein, L., 2020. The rounD dataset: A drone dataset of road user trajectories at roundabouts in Germany. In: 2020 IEEE 23rd International Conference on Intelligent Transportation Systems. ITSC, pp. 1–6.
Krämmer, A., Schöller, C., Gulati, D., Knoll, A., 2019. Providentia-a large scale sensing system for the assistance of autonomous vehicles. In: Robotics: Science and Systems (RSS), Workshop on Scene and Situation Understanding for Autonomous Driving.
Krizhevsky, A., Sutskever, I., Hinton, G.E., 2012. Imagenet classification with deep convolutional neural networks. Adv. Neural Inf. Process. Syst. 25, 1097–1105.
Laval, J.A., Daganzo, C.F., 2006. Lane-changing in traffic streams. Transp. Res. B 40 (3), 251–264.
Laval, J.A., Leclercq, L., 2010. A mechanism to describe the formation and propagation of stop-and-go waves in congested freeway traffic. Phil. Trans. R. Soc. A 368 (1928), 4519–4541.
Li, X., Cui, J., An, S., Parsafard, M., 2014. Stop-and-go traffic analysis: Theoretical properties, environmental impacts and oscillation mitigation. Transp. Res. B 70, 319–339.
Li, L., Jiang, R., He, Z., Chen, X.M., Zhou, X., 2020. Trajectory data-based traffic flow studies: A revisit. Transp. Res. C 114, 225–240.
Lighthill, M.J., Whitham, G.B., 1955. On kinematic waves II. A theory of traffic flow on long crowded roads. Proc. R. Soc. A 229 (1178), 317–345.
Lin, T.-Y., Goyal, P., Girshick, R., He, K., Dollar, P., 2017. Focal loss for dense object detection. In: The IEEE International Conference on Computer Vision. ICCV.
Lin, T.-Y., Maire, M., Belongie, S., Hays, J., Perona, P., Ramanan, D., Dollár, P., Zitnick, C.L., 2014. Microsoft coco: Common objects in context. In: European Conference on Computer Vision. Springer, pp. 740–755.
Luna, E., SanMiguel, J.C., Martínez, J.M., Escudero-Viñolo, M., 2022. Online clustering-based multi-camera vehicle tracking in scenarios with overlapping FOVs. Multimedia Tools Appl. 1–21.
Ma, X., Andréasson, I., 2006. Estimation of driver reaction time from car-following data: Application in evaluation of general motor–type model. Transp. Res. Rec. 1965 (1), 130–141.

Malinovskiy, Y., Wu, Y.-J., Wang, Y., 2009. Video-based vehicle detection and tracking using spatiotemporal maps. Transp. Res. Rec. 2121 (1), 81–89.
May, A.D., 1990. Traffic Flow Fundamentals. Prentice Hall.
Moers, T., Vater, L., Krajewski, R., Bock, J., Zlocki, A., Eckstein, L., 2022. The exiD dataset: A real-world trajectory dataset of highly interactive highway scenarios in Germany. In: 2022 IEEE Intelligent Vehicles Symposium. IV, pp. 958–964.
Montanino, M., Punzo, V., 2015. Trajectory data reconstruction and simulation-based validation against macroscopic traffic patterns. Transp. Res. B 80, 82–106.
Ossen, S., Hoogendoorn, S.P., 2005. Car-following behavior analysis from microscopic trajectory data. Transp. Res. Rec. 1934 (1), 13–21.
Ossen, S., Hoogendoorn, S.P., 2008. Validity of trajectory-based calibration approach of car-following models in presence of measurement errors. Transp. Res. Rec. 2088 (1), 117–125.
Ossen, S., Hoogendoorn, S.P., Gorte, B.G., 2006. Interdriver differences in car-following: A vehicle trajectory–based study. Transp. Res. Rec. 1965 (1), 121–129.
Papageorgiou, M., Diakaki, C., Dinopoulou, V., Kotsialos, A., Wang, Y., 2003. Review of road traffic control strategies. Proc. IEEE 91 (12), 2043–2067.
Parikh, G., Hourdos, J., 2014. Implementation of High Accuracy Radar Detectors for Traffic Safety Countermeasure Evaluation. Center for Transportation Studies, University of Minnesota.
Ray C. Anderson Foundation, 2021. Welcome to The Ray. https://theray.org/technology/. (Online accessed April 2021).
Redmon, J., Divvala, S., Girshick, R., Farhadi, A., 2016. You only look once: Unified, real-time object detection. In: Proceedings of the IEEE Conference on Computer Vision and Pattern Recognition. pp. 779–788.
Ren, X., Wang, D., Laskey, M., Goldberg, K., 2018. Learning traffic behaviors by extracting vehicle trajectories from online video streams. In: 2018 IEEE 14th International Conference on Automation Science and Engineering. CASE, IEEE, pp. 1276–1283.
Roess, R.P., Prassas, E.S., McShane, W.R., 2004. Traffic Engineering. Pearson/Prentice Hall.
Schönhof, M., Helbing, D., 2007. Empirical features of congested traffic states and their implications for traffic modeling. Transp. Sci. 41 (2), 135–166.
Seo, T., Bayen, A.M., Kusakabe, T., Asakura, Y., 2017. Traffic state estimation on highway: A comprehensive survey. Annu. Rev. Control 43, 128–151.
Seo, T., Tago, Y., Shinkai, N., Nakanishi, M., Tanabe, J., Ushirogochi, D., Kanamori, S., Abe, A., Kodama, T., Yoshimura, S., et al., 2020. Evaluation of large-scale complete vehicle trajectories dataset on two kilometers highway segment for one hour duration: Zen Traffic Data. In: 2020 International Symposium on Transportation Data and Modelling.
Shi, X., Zhao, D., Yao, H., Li, X., Hale, D.K., Ghiasi, A., 2021. Video-based trajectory extraction with deep learning for High-Granularity Highway Simulation (HIGH-SIM). Commun. Transp. Res. 1, 100014.
Sochor, J., Špaňhel, J., Herout, A., 2018. Boxcars: Improving fine-grained recognition of vehicles using 3-d bounding boxes in traffic surveillance. IEEE Trans. Intell. Transp. Syst. 20 (1), 97–108.
Spannaus, P., Zechel, P., Lenz, K., 2021. AUTOMATUM DATA: Drone-based highway dataset for the development and validation of automated driving software for research and commercial applications. In: 2021 IEEE Intelligent Vehicles Symposium. IV, IEEE, pp. 1372–1377.
Stern, R.E., Cui, S., Delle Monache, M.L., Bhadani, R., Bunting, M., Churchill, M., Hamilton, N., Pohlmann, H., Wu, F., Piccoli, B., et al., 2018. Dissipation of stop-and-go waves via control of autonomous vehicles: Field experiments. Transp. Res. C 89, 205–221.
Stewart, R., Freeman, M., Taylor, N., Fereday, D., 2006. Highways Agency Active Traffic Management: initial driver reactions to its implementation on the M42. In: Proceedings of the 13th Its World Congress. London, 8–12 October 2006.
Strigel, E., Meissner, D., Dietmayer, K., 2013. Vehicle detection and tracking at intersections by fusing multiple camera views. In: 2013 IEEE Intelligent Vehicles Symposium. IV, IEEE, pp. 882–887.
Subedi, S., Tang, H., 2019. Development of a multiple-camera 3D vehicle tracking system for traffic data collection at intersections. IET Intell. Transp. Syst. 13 (4), 614–621.
Tang, Z., Wang, G., Xiao, H., Zheng, A., Hwang, J.-N., 2018. Single-camera and inter-camera vehicle tracking and 3D speed estimation based on fusion of visual and semantic features. In: Proceedings of the IEEE Conference on Computer Vision and Pattern Recognition Workshops. pp. 108–115.
Tennessee Department of Transportation, 2022. Annual Average Daily Traffic (AADT) Maps. https://tdot.ms2soft.com/tcds. (Online accessed December 2022).
Tordeux, A., Lassarre, S., Roussignol, M., 2010. An adaptive time gap car-following model. Transp. Res. B 44 (8–9), 1115–1131.
Treiber, M., Hennecke, A., Helbing, D., 2000. Congested traffic states in empirical observations and microscopic simulations. Phys. Rev. E 62 (2), 1805.
Treiber, M., Kesting, A., Helbing, D., 2010. Three-phase traffic theory and two-phase models with a fundamental diagram in the light of empirical stylized facts. Transp. Res. B 44 (8–9), 983–1000.
Treiterer, J., Myers, J., 1974. The hysteresis phenomenon in traffic flow. Transp. Traffic Theory 6, 13–38.
Turner, D.S., 2011. 75 Years of the Fundamental Diagram for Traffic Flow Theory: Greenshields Symposium: July 8-10, 2008, Woods Hole, Massachusetts. Transportation Research Board.
University of Michigan Engineering, 2021. About Ann Arbor Connected Vehicle Test Environment (AACVTE). https://aacvte.engin.umich.edu. (Online Accessed April 2021).
von Schmidt, A., López Díaz, M., Schengen, A., 2021. Creating a baseline scenario for simulating travel demand: A case study for preparing the region test Bed Lower Saxony, Germany. In: International Conference on Advances in System Simulation. SIMUL, ThinkMind, pp. 51–57.
Wang, Y., Gloudemans, D., Teoh, Z.N., Liu, L., Zachár, G., Barbour, W., Work, D., 2022. Automatic vehicle trajectory data reconstruction at scale.
Wu, M., Zhang, G., Bi, N., Xie, L., Hu, Y., Shi, Z., 2019. Multiview vehicle tracking by graph matching model. In: CVPR Workshops. pp. 29–36.
Yeo, H., Skabardonis, A., 2009. Understanding stop-and-go traffic in view of asymmetric traffic theory. In: Transportation and Traffic Theory 2009: Golden Jubilee. Springer, pp. 99–115.
Zhan, W., Sun, L., Wang, D., Shi, H., Clausse, A., Naumann, M., Kummerle, J., Konigshof, H., Stiller, C., de La Fortelle, A., et al., 2019. Interaction dataset: An international, adversarial and cooperative motion dataset in interactive driving scenarios with semantic maps. arXiv preprint arXiv:1910.03088.
Zhang, T., Jin, P.J., 2019. A longitudinal scanline based vehicle trajectory reconstruction method for high-angle traffic video. Transp. Res. C 103, 104–128.
Zhao, D., Li, X., 2019. Real-world trajectory extraction from aerial videos-a comprehensive and effective solution. In: 2019 IEEE Intelligent Transportation Systems Conference. ITSC, IEEE, pp. 2854–2859.
Zheng, O., Abdel-Aty, M., Yue, L., Abdelraouf, A., Wang, Z., Mahmoud, N., 2022. CitySim: A drone-based vehicle trajectory dataset for safety oriented research and digital twins. arXiv preprint arXiv:2208.11036.
Zheng, Z., Ahn, S., Chen, D., Laval, J., 2011. Applications of wavelet transform for analysis of freeway traffic: Bottlenecks, transient traffic, and traffic oscillations. Transp. Res. B 45 (2), 372–384.
Zielke, B.A., Bertini, R.L., Treiber, M., 2008. Empirical measurement of freeway oscillation characteristics. Transp. Res. Rec. J. Transp. Res. Board 2088, 57–67.